Master's Thesis

Master in Telecommunication Engineering

Characterization of Starlink constellation

Pol Pérez Rodríguez

Thesis Advisor: Maria Ángeles Vázquez Castro

Department of Telecommunications and Systems Engineering

Escola d'Enginyeria (EE)

Universitat Autònoma de Barcelona

Bellaterra, February 2022

El sotasignant, Maria Ángeles Vázquez Castro, Professor de l'Escola d'Enginyeria (EE) de la Universitat

Autònoma de Barcelona (UAB).

CERTIFICA:

Que el projecte presentat en aquesta memòria de Treball Fi de Máster ha estat realitzat sota la seva direcció per l'alumne Pol Pérez Rodríguez.

I, perquè consti a tots els efectes, signa el present certificat.

Bellaterra, Febrer de 2022.

Signatura:

Resumen: La constelación Starlink, que actualmente cuenta con un total de 1693 satélites, puede parecer una solución novedosa al problema de las comunicaciones en todas las regiones del mundo, pero no fue la primera en aparecer en nuestros cielos como podremos ver en el trabajo, observando las principales características de las constelaciones que existen actualmente. En este artículo únicamente analizaremos técnicamente la constelación Starlink, examinando cada uno de los satélites actualmente en órbita y observando los parámetros habituales de un sistema de radiocomunicación tierra-satélite. Se discutirá la geometría orbital y se mostrará el modelo matemático correspondiente a este enlace. En este enlace se realizará un análisis exhaustivo de las pérdidas de atenuación en los estándares de comunicación, y se comprobará hasta qué punto la capacidad de canal propuesta por Space X se asemejan a la realidad; tanto en puntos discretos como en un estudio posicional a nivel global, proporcionando una primera visión general del sistema.

Resum: La constel · lació Starlink, que actualment compta amb un total de 1693 satèl · lits, pot semblar una solució nova al problema de les comunicacions a totes les regions del món, però no va ser la primera a aparèixer al nostre cel com podrem veure a la feina, observant les principals característiques de les constel · lacions que existeixen actualment. En aquest article únicament analitzarem tècnicament la constel · lació Starlink, examinant cadascun dels satèl · lits actualment en òrbita i observant els paràmetres habituals d'un sistema de radiocomunicació terra-satèl · lit. Es discutirà la geometria orbital i es mostrarà el model matemàtic corresponent a aquest enllaç. En aquest enllaç es realitzarà una anàlisi exhaustiva de les pèrdues d'atenuació als estàndards de comunicació, i es comprovarà fins a quin punt la capacitat de canal proposada per Space X s'assemblen a la realitat; tant en punts discrets com en un estudi posicional a nivell global, proporcionant una primera visió general del sistema

Summary: The Starlink constellation, which currently has a total of 1693 satellites, may seem like a novel solution to the problem of communications in all regions of the world, but it was not the first to appear in our skies, as we will see in the paper, looking at the main characteristics of the constellations that currently exist. In this article we will only technically analyse the Starlink constellation, examining each of the satellites currently in orbit and looking at the usual parameters of a ground-to-satellite radio communication system. The orbital geometry will be discussed and the mathematical model for this link will be shown. This link will provide an exhaustive analysis of the attenuation losses in the communication standards, and will check to what extent the channel capacity proposed by Space X resembles reality; both in discrete points and in a global positional study, providing a first overview of the system.

Contents

List of Figures

List of Tables

Chapter 1

Introduction

Historically, there has always been a desire to obtain great control over space and its communications, a great engineering challenge with very high costs that lead to an early death of the different projects that wanted to establish themselves as a reference in this field. Many have tried, and very few have managed to achieve the transmission capacity and coverage that they promised in their beginnings.

In this context, Space X, with its Starlink project, wants to revolutionise the concept of constellations by taking the definition of constellations to the extreme, with the idea of including more than 12,000 satellites in LEO orbit by the end of the 2020s. To do this, without losing sight of the fact that it is a business, led by CEO Elon Musk, they have created a reusable rocket that minimises launch costs, together with a nanosatellite design, and this constellation is expected to be a great success. For now, the first version has more than 1,500 functional satellites in orbit, giving a first glimpse of what it could look like.

So, in this study will validate this assertion and provide examples in order to characterize the different parameters of a satellite telecommunications system. To do so, we will study the 1693 [21] satellites, giving a first approximation of the power of this mega constellation in LEO orbit.

The losses of a communication link will also be analysed according to the different ITU's, such as losses due to rain or clouds. This analysis will be described following all the variable parameters that have the atmospheric losses, giving us the ability to understand the importance of losses within the communication link with the satellite.

1.1 Motivation

SpaceX, led by its CEO Elon Musk, has promised great feats for this mega constellation, capabilities that need to be studied and considered analytically, in order to get the reality of the basic characteristics of these satellites.

The primary motivation is to analyze the design of the constellation to check what is the actual target coverage (at least for now). Based on such analysis, we would like to obtain communication performance metrics and check whether or not they match promised rates.

Secondly, another motivation is to apply the different skills learnt during the academic period to provide an effective solution for processing data from a constellation of this magnitude. This will require a combination of data analysis skills, data processing and knowledge of radio frequency links, leading to a complete understanding of the losses or phenomena included in the study.

1.2 Objectives and methodology

The main objective of this work is the characterization of the Starlink constellations and Internet service from capacity point of view. Towards such aim, first of all we perform a comprehensive analysis of the constellation from orbit geometry. This study then allows us to compute and analyze the communication capacity and corresponding geo-spatial variability.

The sub-objectives in order to obtain the final results, the following have been stated:

- Understanding TLE files.
- Software capable of analysing the data.
- Thorough analysis of attenuation losses in communication standards.
- Obtaining total constellation capacities from different points in the world.

The methodology of the work will be divided according to the following points:

- Analysis of the published literature.
- Characterization of the constellation through the development of Matlab functions.
- Computation and analysis of capacity and statistical variability depending on the geo-spatical target coverage.

1.3 Document structure

The structure of the document will serve as follows, divided into the chapters described below.

- Chapter 2: This chapter focuses on a historical and current overview of the different constellations. It also looks at the different orbits that exist.
- Chapter 3: This chapter considers the mathematical model to be used in the analysis of the system.
- Chapter 4: In this chapter the Starlink constellation will be analysed with variations in the parameters of the system.
- Chapter 5: In this chapter the capacity of the system will be shown together with the associated losses that it will have.
- Chapter 6: conclusions of the study.

Chapter 2

Background and state of art

This second chapter will deal with the explanation and study of the art of the project, with its historical and motivational concept.

Then, in this chapter we will analyze historically the most outstanding constellations that have existed as well as the problems they may have had. Finally, we will comment on the current situation, with emphasis on the constellation of study of this work, Starlink.

2.1 Historical constellations

2.1.1 Teledesic

Teledesic was a company founded in the 1990s, the major shareholders being Craig McCraw, founder of McCaw Cellular Communications; and Microsoft owner Bill Gates [25].

Initially, it was a broadband communication with terrestrial support in the form of fibre optics. The main motivation of this constellation was to be able to provide internet in all rural areas of the world. Initially, this concept was to be realized by 924 satellites in Low-Earth Orbit (hereafter LEO) in the Ka band. The Teledesic satellite uplink operate in the 30 GHz band and 20 GHz band for the downlink.

It should be noted that Teledesic had other purposes within its operation, for example:

- Bit error rate.
- Geodesic network interconnect.
- High data rate.

– Low latency.

Typically, in a LEO constellation we have a latency of 20 microsec. The reason for choosing LEO orbit is because of its proximity to the earth, which means minimal latency, as we would not have, for example, in geostationary orbit, with a minimum communication latency of 500 microsec. On the other hand, we will have a considerable reduction in the useful life of the satellites in orbit.

To satisfy the interconnection with high data throughput, with few failures, it was necessary to have a mesh of satellites to pass the data in a concrete way and with the ability to change the packet path with little difficulty. and with the ability to change the path of packets with little difficulty. This was done by orbiting 21 orbits between 695 and 705 kilometres, described in the figure 2.1. Each of these planes is composed of 40 satellites. On the part of the operation working the constellation and to have a good

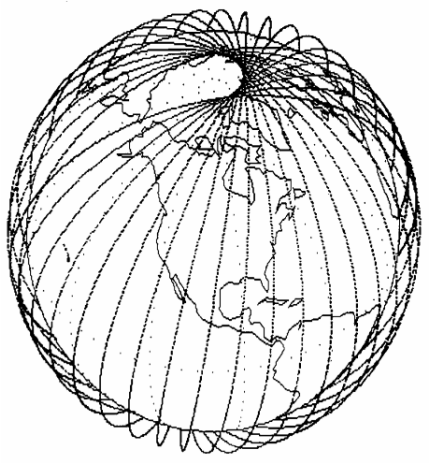

Figure 2.1: Teledesic orbits. [1]

communication it used an access coordination:

– Space division.

– Time division.

– Frequency division.

This was done to ensure efficient use of the operating spectrum.

2.1.2 Iridium

Continuing with the same idea of historical context, we come across another constellation of satellites, named Iridium of American origin. Curiously, this name is given by the chemical element Iridium, being the 77th element of the periodic table; and at the same

time, the number of satellites that this constellation wanted to have; right now we fear 66 in orbit [2]. Note that this constellation is in LEO since the same latency conditions are required as in the previous case.

In this constellation, we can see that it has a different purpose than the previous one. In this case, Motorola, an American telecommunications company, wanted to provide data for voice communication and interconnection using portable devices in areas with complex or minimal coverage. This, in effect, set them apart from traditional telephony such as landline or cellular. About the technical considerations, as we can see in the

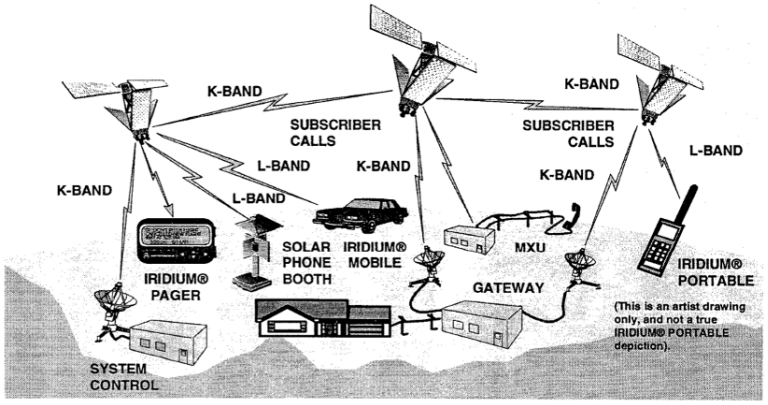

Figure 2.2: System overview of Iridium. [2]

previous diagram, figure 2.2, the communications between the antennas and the satellites are with K-Band (18-27 GHz); as far as communication to mobile devices is concerned, we are afraid of the L-Band (1-2 GHz). Finally, the bandwidth used for communications has a value of 5.15 MHz [2].

In terms of how the information is packaged between the links, there are two types:

- TDMA for links to mobile devices.
- TDMA/ FDMA for links between satellites.

2.1.3 Globalstar

In this case, Globalstar Inc. is again a telecommunications company that has 66 satellites in low LEO orbits, with an altitude of approximately 780 kilometres from the earth.

These satellites are distributed in 6 orbits of 11 satellites, equidistantly distributed. As in the previous case, this constellation with a telephonic purpose was designed by Motorola.

In a second generation of these satellites, 24 more satellites have been sent into orbit; also in low LEO orbit.

At a technical level, this constellation has an inclination of 52 degrees above the earth; a characteristic that does not give it the capacity to cover the polar zones, since it has a very small angle. Similar to the value obtained by the constellation under study, Starlink, with a value of 53º. [19]

As we can see in figure 2.3, and corroborating with the statement described above, we observe that the coverage disappears at the poles of the earth. In orange colour, we can easily see where we will have a principal coverage, being in grey, the weakest signal.

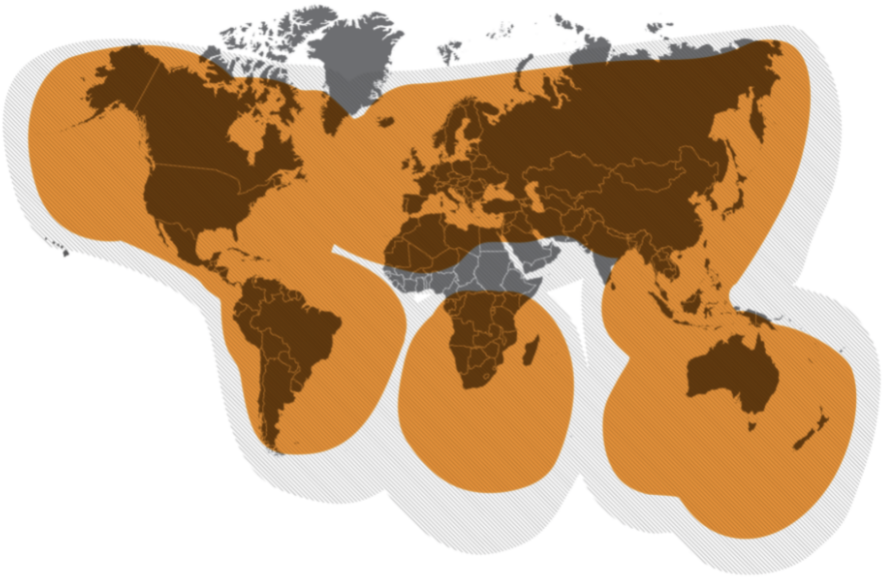

Figure 2.3: Globalstar coverage. [3]

As far as latency is concerned, we have a relatively low value, being 60 ms the average of the communication.

Emphasizing the modulation of the communication between the satellites and the client, we know that it is Frequency Division Spread Spectrum CDMA providing an optimal and flexible service to the user. The FD/SS/CDMA modulation gives the ability to have several satellites with different paths, having less fading and service blockages.

As mentioned above, two generations of satellites have been launched into orbit, the first

ones having problems in the S-band amplifiers (2 - 4 GHz), causing poor communication, leading to poor compatibility at the time of bidirectional communication (to the client). This problem led Globalstar to send 24 satellites in a second generation, considering the problems encountered in the first generation. This second batch led to a significant increase in the useful life of the satellites (from 7.5 years to 15).

2.1.4 ORBCOMM

Finally, on a historical level, the ORBCOMM constellation should be mentioned. This constellation is owned by an American company, named after the constellation. It currently has approximately 50 satellites in low LEO orbit.

The peculiarity of this constellation is that it is a generation that is used for M2M (machine to machine) communication; it is the first one that has a different target than telephony users.

Figure 2.4: Orbcomm M2M. [4]

This constellation, in particular the ORBCOMM-OG2 generation (after ORBCOMM-OG1, now deprecated), uses the Very High Frequency (VHF) frequency, between 30 to 300 MHz. The choice of this communication band implies an increase in signal propagation and a minimal impact of bad weather on the BER.

At the technical level, we know that the frequency of use is as follows:

- 148-150,05 MHz for user and gateway links.
- 400.1 MHz for user downlink.
- 137-138 MHz for gateway and user downlinks.

2.2 State of art

Once we have commented on the different historical constellations we have had, with their different purposes and technical concepts, we are going to make a sweep of the current constellations that are being created. To do so, we will comment on the main competitors of the protagonist of this work, Starlink.

2.2.1 OneWeb

One of the main competitors for the Starlink constellation is One Web, an English company owned by Airbus Defense and Space, founded in 2012 and declared bankrupt in 2020 due to the Coronavirus. Currently, it is still waiting to continue the creation of the constellation, due to budget problems.

The main idea of this company was to create a constellation of 650 satellites divided into 18 planes, for the purpose of satellite internet access, covering all areas of the planet.

These satellites were prepared to operate in LEO at an altitude of 1200 km above the earth, because there is a minimal population of satellites and space debris at that altitude. It should also be noted that they continue to choose this orbit because they are looking for low latency, high bandwidth; a problem solved in geostationary orbit. They also wanted to include another constellation in MEO, of 1280 satellites.

Figure 2.5: OneWeb satelite model. [5]

One of the novelties compared to other previously mentioned constellations is that these satellites have a lifetime of 5 to 7 years, but at the end of their life, they leave their orbit

and disappear as they come in towards the Earth. As we can see in the figure 2.5, the size is relatively small giving this possibility.

The satellites will operate in the Ku-band (12 - 18 GHz); given the potential for interference with GEO satellites operating in the same band, the OneWeb satellites have the ability to operate intermittently and rotate their position slightly, mitigating these potential errors. As far as the link to the customer is concerned (downlink), it is considered to be about 50 Mbit/s.

2.2.2 Other competidors

In this list, we can put a couple of major competitors, which have not yet been able to create their respective constellations, being Amazon, with its Kuiper project, or the large Chinese constellation, Guowang, consisting of more than 13,000 functional satellites.

First of all, as far as Amazon and the Kuiper project are concerned, although not much information is known yet, we know that it will consist of some 3,300 satellites in LEO orbit, spread over nine launches with Atlas V rockets.

On the technical and economic side, a considerable increase in communication speed over Starlink is promised, with a maximum throughput of 400 Mbps, almost twice the speed promised by Starlink. As for the working band, it will be Ka-band. It is also worth mentioning that the antennas designed by amazon will have a smaller size, resulting in less hardware and a reduction in the price of the service. This second point is one of the most tantalising about this new constellation in its embryonic stage.

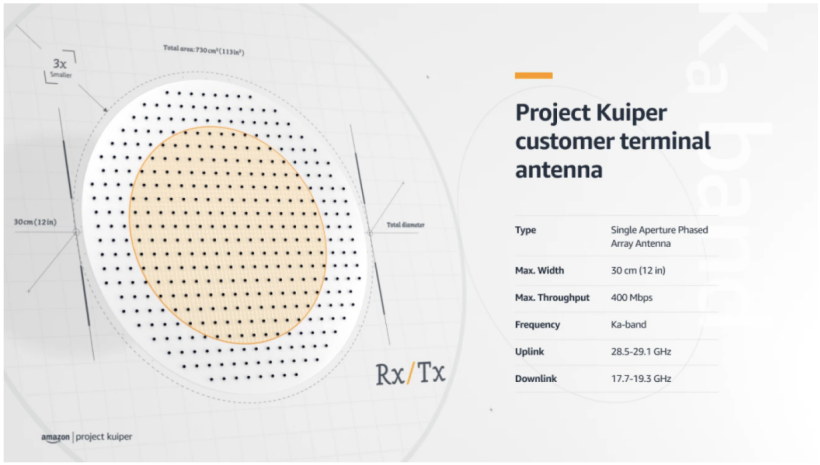

Figure 2.6: Configuration of the Tx/Rx antenna. [6]

As we can see in the figure 2.6, we have the emitting and transmitting antenna, a very

important achievement given the operating band.

Historically, there have been many problems in creating this type of antenna in Ka-band (in Ku-band, there is no problem), due to the fact that the transmission (18-20 GHz) and reception (28-30 GHz) frequencies are very far apart, which means that the antenna aperture is not sufficient to combine both communications.

The solution Amazon's engineers have come up with is to create a kind of radiation system where multiple antennas have the same aperture. This array of antennas creates a focused beam at the frequencies of interest. This is a major breakthrough in radio frequency because it has never been possible before.

On the other hand, we have the Chinese project with the plan to create two constellations (GW-A59 and GW-2), with a total of 13,000 satellites.

Although the purpose will be the same as Starlink, it will also have a military focus; detecting nuclear missiles and creating communication channels between aircraft and ground vehicles.

2.2.3 Starlink

Finally, we have Starlink, the reason for the study of this thesis, being a company that was born as a project of SpaceX, having the same purposes that we have discussed above of the competitors, but also with its sights set on a future on another planet, Mars.

As far as the use of satellites is concerned, you will have three major buyers:

- Military use.
- Scientific use.
- Exploration use.

The approval of the various launches and permits related to the project was divided into different batches. A series of 4,425 satellites, functional in Ka- and Ku-band, were initially approved. These would be in the LEO orbit, characterized by low latency. This first set of satellites will orbit at 340 kilometres.

In a second proposal, around March 2017, the satellites will be located in the V-band (40 - 75 GHz), in non-geosynchronous orbits, i.e. in non-geocentric orbits. Therefore, the second constellation proposal will be in the VLEO orbit, consisting of

7,518 satellites. These satellites were originally intended to operate in 83 orbital planes, at altitudes between 1,110 and 1,325 km. In view of space contamination, this altitude was moved to 550 km, slightly above the first ones.

In terms of frequency and equipment operation, optical links will be used for communication with each other, and digital beam antennas in the Ku and Ka bands.

In terms of communication latency, Starlink expects latencies to be between 7 and 30 ms, which is lower than existing fibre.

As far as download speed is concerned, there is a growing trend in this data, given that there is more and more equipment in orbit. Initially, they had a value of 94 Mbps, although they promise a higher one than conventional fibre, being 115 Mbps.

Given the promises made by the SpaceX company and taking into account its technical characteristics, the motivation for this project is clear: to seek the limits of the system and to observe to what extent the different technical characteristics they indicate are possible. Also, to know to what extent we can deny or increase the capabilities of the channel in question. To do this, we will have to be very clear about the technical and geometrical considerations of our planet and to obtain numerical comparisons in order to contrast the certain objectives.

2.3 Types of orbits

From the future sections, we are going to see that we can easily characterize any element that orbits the earth thanks to the TLE files. In the figure 2.7, we can observe the different coverage between the typical orbits in the Earth; in addition, we can observe also the distance of the satellite to the Earth.

2.3.1 Geostationary Orbit (GEO)

As far as the GEO orbit is concerned, we know that they orbit about 35,786 kilometres above the Earth's equator. This altitude gives an approximate period of 24 hours (23 hours 56 minutes and 4 seconds), which means that they are always in the same place.

Knowing that their position is constant, they must have full coverage over the Earth's surface, having a latency of approximately 0.24 seconds. [26]

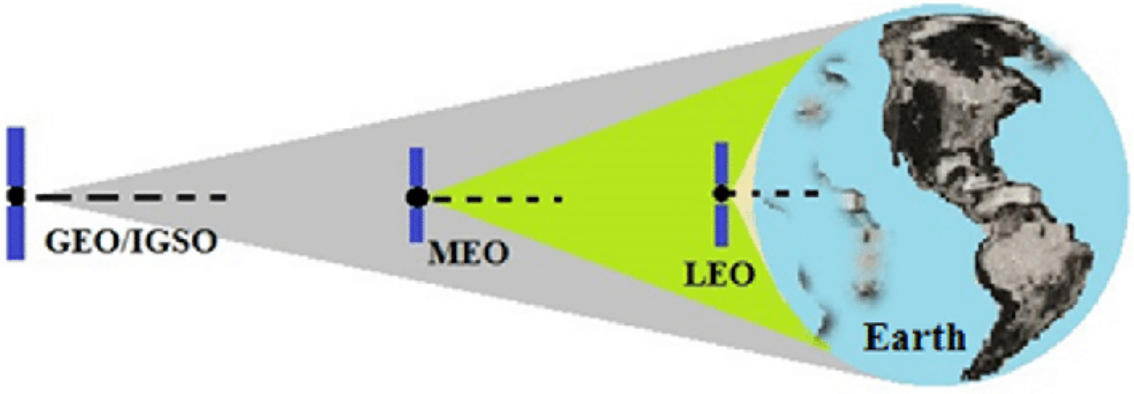

Figure 2.7: Comparison between the different orbits. [7]

2.3.2 Low Earth orbit (LEO)

Secondly, LEO orbits are low altitude orbits with a very high bandwidth, resulting in low latency. The altitude is usually below 1000 kilometres, although they can be up to 160 kilometres above the earth.

Three types of LEOs handle different amounts of bandwidth. Small LEOs are intended for low bandwidth applications (tens to hundreds of Kbps), such as paging, and include systems such as OrbComm. Large LEOs can handle paging, mobile phone services and some data transmission (hundreds to thousands of Kbps). Wideband LEOs (also called megaLEOs) operate in the Mbps range and include Teledesic, Celestri and SkyBridge.

Unlike satellites in GEO that must always orbit along Earth's equator, LEO satellites do not always have to follow a particular path around Earth in the same way – their plane can be tilted. This means there are more available routes for satellites in LEO, which is one of the reasons why LEO is a very commonly used orbit. [26]

2.3.3 Medium Earth orbit (MEO)

Medium earth orbit satellites are located at an altitude between 10075 and 20150 kilometres. Unlike GEO satellites, their position relative to the surface is not fixed. Being at a lower altitude, more satellites are needed to obtain global coverage, but latency is substantially reduced. At present, there are not many MEO satellites, and they are used for positioning. [26]

Chapter 3

Geometric model

In this chapter, the different orbital parameters of a satellite will be explained from a mathematical and theoretical point of view; the origin of these parameters will also be explained.

The format of the files where the data for the study have been collected, being the TLE files, will be shown. In addition, the step-by-step procedure for obtaining each of the points under study in this work will be shown.

3.1 Orbits

The path that a satellite follows is called an orbit. There can be multiple orbits around a celestial object, so a standard way to specify an orbit is to know what are called the orbital elements. The traditional ones are the six Keplerian elements:

- Three for the spatial dimensions.
- Three for the velocities.

These elements can be seen in the figure 3.1 together with the orbital plane of the satellite itself. These elements will be key to be able to obtain all the information from all the satellites in the constellation. The parameters are described below:

- Semi-major axis (a): The semi-major axis is the longest semi-diameter or half of the major axis and therefore extends from the centre through a focus to the perimeter. The unit of this parameter is metres [m].
- Eccentricity (e): This parameter is about the shape of the orbit in question. When we have an eccentricity equal to 0, we have a perfect circle around the Earth. In the case of having a value between 0 and 1 ($0 \leq e \leq 1$), it is an elliptical orbit, leading to

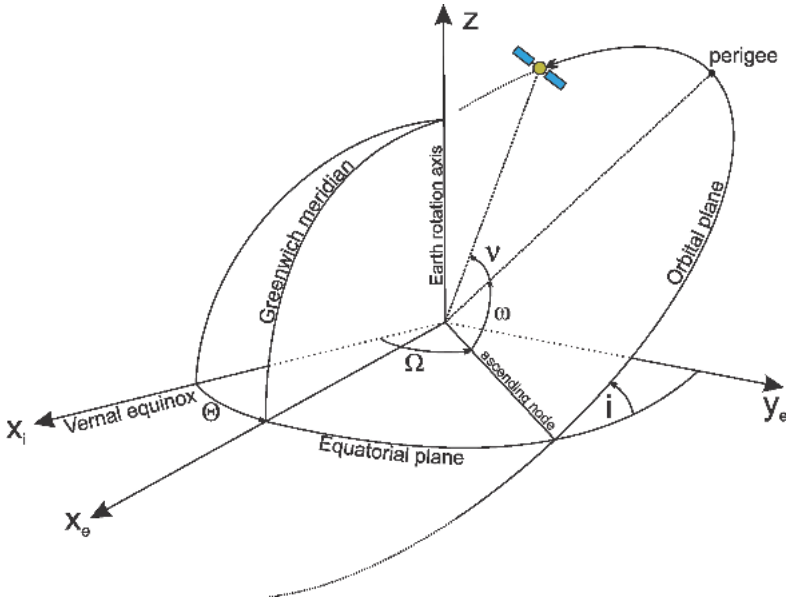

Figure 3.1: Keplerian elements. [8]

a variation in the distance of the satellite from the earth. In this case, they do not have any unit.

- Inclination (i): is the angle of the orbit relative to the earth's equator. So, for example, having a satellite orbiting from the north pole, towards the south pole, we will have an inclination of 90 degrees. Therefore, the units are degrees [°].
- Argument of periapsis (ω): defines the orientation of the ellipse within the orbital plane; the units may be radians [rad] or degrees [°].
- True anomaly (v): is the position of the body within the orbit, for a given time. The unit is seconds [s].
- Right ascension (or longitude) of the ascending node (Ω):horizontally orients the ascending node of the ellipse (where the orbit passes upward through the reference plane) with respect to the reference frame's vernal point.

3.1.1 TLE element

As mentioned above, we have a number of parameters, which can be calculated in different ways. For our case, being the most common, we will use the two-line element set (TLE). The TLE is a file with data for an element orbiting the earth, for a certain time, the epoch. The configuration of this file is based on 3 lines of 70 columns.

Taking one of the rows of the Starlink TLE file, obtained in [21]:

```
STARLINK-1007
```

```
1 44713C 19074A   21342.44742259  .00009133  00000-0  61198-3 0  3425
2 44713  53.0499 314.9290 0002108  55.0531 161.5272 15.06384893    11
```

For clarity, the tables 3.1 and 3.2; where the fields, columns, content and value within the example will be described, are added. All this for line two and three, because the first one only marks the name of the satellite to which the subsequent information belongs.

Field	Columns	Content	Example
1	1	Line Number	1
2	3-7	Satellite Number	44713
3	8	Classification	C
4	10-11	International Designator (Last two digits of launch year)	19
5	12-14	International Designator (Launch number of the year)	074
6	15-17	International Designator (piece of the launch)	A
7	19-20	Epoch Year (last two digits of year)	21
8	21-32	Epoch (day of the year and fractional portion of the day)	342.44742259
9	34-43	First time derivative of the Mean Motion divided by two	.00009133
10	45-52	Second time derivative of MM divided by six	00000-0
11	54-61	BSTAR drag term	61198-3
12	63	The number 0 (”Ephemeris type”)	0
13	65-68	Element set number.	342
14	69	Checksum	5

Table 3.1: Parameters of the first TLE line.

Note that all the parameters necessary for the development of these tesis are highlighted at the previous tables.

The most important parameters in the first line are the Epoch Year and Epoch, which refer to the time at which the satellite data is retrieved. With these values, we can retrieve the exact moment where the satellite is in its orbit.

As a curiosity, the Epoch Year parameter is described with two digits, giving the possibility of confusion in the future: for example, with an Epoch Year of 60, we could be in 2060 or 1960. Therefore, the modification of this field to three digits is being considered. However, for the time being, all values greater than 0, up to the current year, are treated as 21st century.

On the Epoch side, this is the sum of days that have passed up to the date of the

Field	Columns	Content	Example
1	1	Line number	2
2	2-7	Satelilte number	44713
3	9- 16	Inclination (degrees)	53.0499
4	18-25	Right ascension of the ascending node (degrees)	314.9290
5	27-33	Eccentricity (decimal point assumed)	0002108
6	35-42	Argument of perigee (degrees)	55.0531
7	44-51	Mean Anomaly (degrees)	161.5272
8	53-63	Mean Motion (revolutions per day)	15.06384893
9	64-68	Revolution number at epoch (revolutions)	1
10	69	Checksum	1

Table 3.2: Parameters of the second TLE line.

file. The decimals describe the proportional part of the current day. In order to determine the exact time of the current day, the following procedure is followed:

```
342.44742259  --> 342 days
0.44742259*24 --> 10.7381 hours
0.7381*60     --> 44.2885 min
0.2885*60     --> 17.3118 seg
```

Therefore, the values described in this example are from 20 November 2021, at 10:44 a.m.

On the second line of the TLE file, we have all the orbital parameters necessary to correctly describe the motion of our celestial body.

3.2 Calculation of the ground track

As explained the orbital parameters in the 3.1 section, they will be necessary to calculate the different satellite coordinates, to obtain the satellite's ground track and to obtain the visibility time for a terrestrial point.

In the figure 3.2, we can see the orbital parameters described for the LEO orbit, being the orbit of interest for our study. First, we must be clear about the initial distance of our satellite, given by the following equation [16]:

$$r_0 = a(1 - e\cos E) \tag{3.1}$$

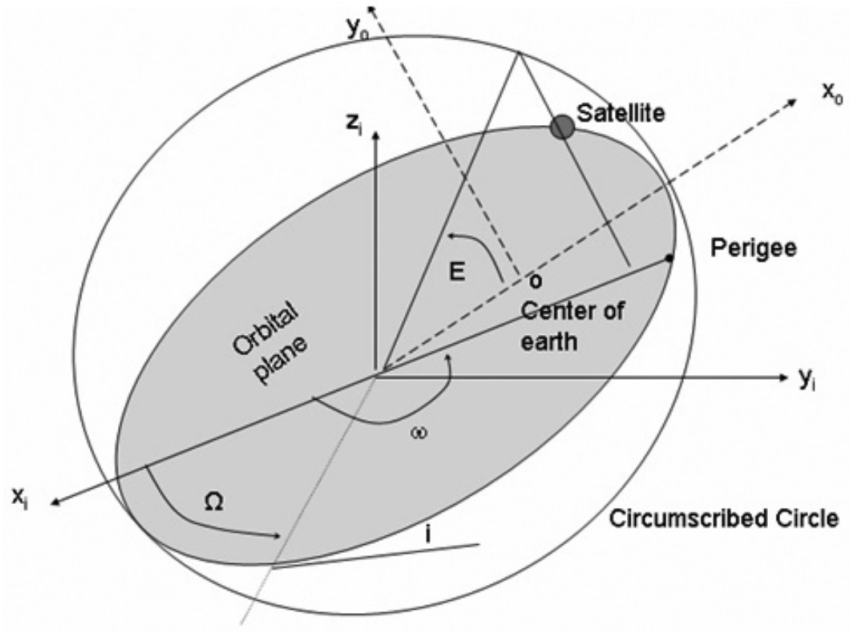

Figure 3.2: LEO Satellite Parameters. [16]

Where E is the eccentric anomaly, which is related to M as: [16]

$$M = E - e \sin E \tag{3.2}$$

Given that in the LEO orbits we have an e≤0.001, we can consider that M ≈ E.
From the initial Cartesian coordinates, we will have the following vector:

$$\begin{bmatrix} x_o \\ y_o \\ z_o \end{bmatrix} = \begin{bmatrix} r_0 \cos v \\ r_0 \sin v \\ 0 \end{bmatrix} \tag{3.3}$$

Where v, is the true anomaly, extracted in the TLE data described before. Next, we must modify the Cartesian coordinates, towards the Earth Centered Inertial (ECI) coordinate, giving rise to a rotation around z_0, placing the x_0 axis in the equatorial plane (ω). For this purpose, the equation 3.4 will be used.

$$\begin{bmatrix} x_i \\ y_i \\ z_i \end{bmatrix} = R_{eci} \begin{bmatrix} x_o \\ y_o \\ z_o \end{bmatrix} \tag{3.4}$$

Where R_{eci} is given by [10]:

$$R_{eci} = \begin{bmatrix} \cos\omega\cos\Omega - \sin\omega\cos i\sin\Omega & -\sin\omega\cos\Omega - \cos\omega\cos i\sin\Omega & \sin\Omega\sin i \\ \cos\omega\sin\Omega + \sin\omega\cos i\cos\Omega & -\sin\omega\sin\Omega + \cos\omega\cos i\cos\Omega & -\cos\Omega\sin i \\ \sin\omega\sin i & \cos\omega\sin i & \cos i \end{bmatrix} \tag{3.5}$$

In order to arrive at the final value of the rotation matrix R_{eci}, the following steps have been carried out:

- Rotation around Z_0, being perpendicular to the orbit. Placing the X_0 axis in the equatorial plane. This motion creates a vector called r_1, composed of x_1,y_1 and z_1.
- The second step, we will have a rotation in the x-component (x_1) of the previously mentioned vector. This procedure converts the Z axis into the polar axis and also creates a new plane $x_1' - y_1'$, on the equatorial plane.
- Finally, having this new plane, named r_1'; we will only have to align the x-axis, in the direction of the vernal point or ascending node longitude.

All of these values are described within the TLE file, discussed in the section 3.1.1.

Once we have the ECI coordinates, we must include the time factor into the equation. To do this, we will take our inertial coordinates, into the rotational coordinates, noted as:

$$r_r = \begin{bmatrix} x_r \\ y_r \\ z_r \end{bmatrix} \tag{3.6}$$

For the calculation of these new coordinates, described in the figure 3.7, we can see that they have to be related to the Earth's rotation speed (Ω_e) and the time elapsed (T_e) since $x_r = x_i$. Focusing in the time lapsed (T_e), we will need to obtain the Julian Date (JD) of the initial time of the satellite(t_0).

Julian Date is simply a way of naming moments, and it's simpler than the usual date and time system. Usually, to determine the date and time, you need six different numbers - year, month, day, hour, minute, and second - and comparing two dates is terrible math, with some added complexity. Because some months have 30 days, others have 31 days, for example. The Julian date specifies a simple floating point number for each calendar date as well as the time and is much easier to use. Cabe comentar también que en algunos casos, es algo complicado el cálculo del JD, por lo tanto, muchas veces se calcula el Reduced Julian Date (RJD), teniendo la equivalencia descrita en la ecuación 3.8a.

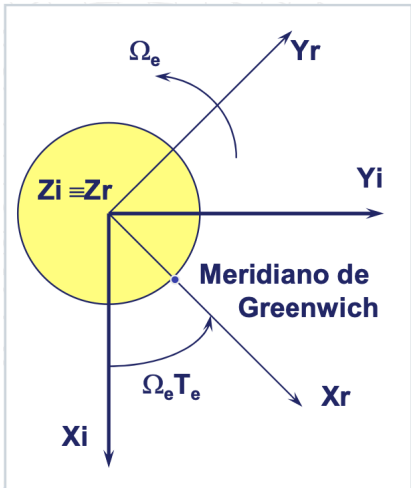

Figure 3.3: Description of the inertial and rotational coordinates. [11]

Entonces, la forma de calcular el JD, la podemos realizar de la siguiente manera:

$$JD = 2451544,5 + 365Y + 0,25Y - 0,01Y + 0,0025Y + A + D + \frac{1}{24}H + \frac{1}{1441}M + \frac{1}{86400}S \tag{3.7}$$

where:

- Y =Year
- A = is a correction factor. If the year is a leap year, it is -1, otherwise it is zero.
- D = Days
- H = Hours
- M = Minutes
- S = Seconds

The following code in Matlab, calculus the JD and RJD [23]:

```
[Year,Month,Day,H,M,S] = datevec(OE.epoch);
HourUTC = H + M/60.0 + S/3600.0;
jd = 2451544.5 + 365*Year + 0.25 * Year - 0.01 * Year + 0.0025* Year + ...
    Day + H/24 + M/1441 + S/86400;
jd0 = 2451544.5 + 365*Year + 0.25 * Year - 0.01 * Year + 0.0025* Year + ...
    Day ;
rjd = (jd - 2451545);
T = rjd/36525;
```

Once the JD is calculated, we can proceed to calculate the RJD and finally the Greenwich Meridian Sidereal Time (GMST) being the measure of the earth's rotation with respect

to distant celestial objects.

These parameters can be easily extracted with the expressions [18] below:

$$RJD = JD - 2451545.0 \tag{3.8a}$$

$$T = RJD/36525 \tag{3.8b}$$

$$GMST[s] = 24110.54841 + 8640184.812866T + 0.093104T^2 - 0.0000062T^3 \tag{3.9}$$

Once all the above has been calculated, we can make the relation between coordinates with the following expression:

$$\begin{bmatrix} \mathrm{x_S} \\ \mathrm{y_s} \\ \mathrm{z_S} \end{bmatrix} = \mathrm{R_r} \begin{bmatrix} \mathrm{x_r} \\ \mathrm{y_r} \\ \mathrm{z_r} \end{bmatrix} \tag{3.10}$$

where R_r [16]:

$$R_r = \begin{bmatrix} \cos(GMST) & \sin(GMST) & 0 \\ -\sin(GMST) & \cos(GMST) & 0 \\ 0 & 0 & 1 \end{bmatrix} \tag{3.11}$$

In figure 3.4, we can see the orbits of a set of 1000 satellites of the Starlink constellation. As we can easily see, one of the characteristics of this constellation is that it does not have

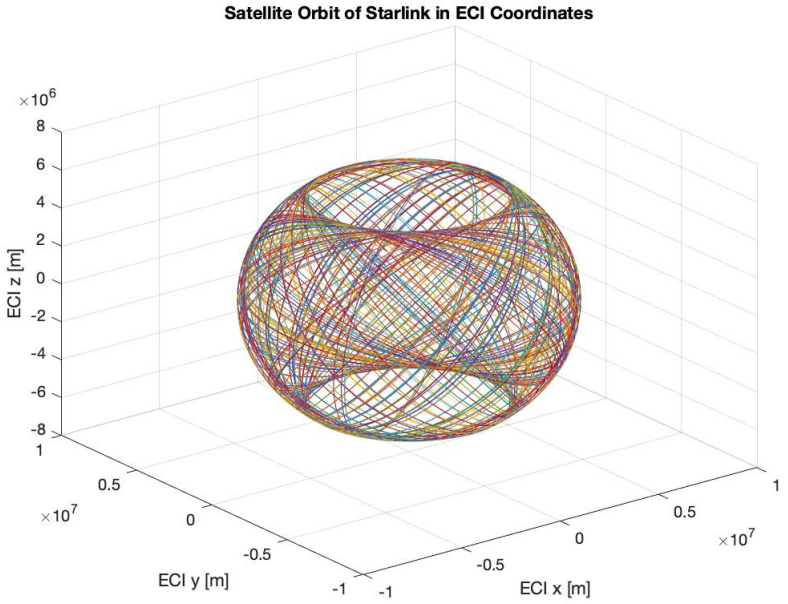

Figure 3.4: Orbits of 1000 Starlink satellites.

coverage within the Earth's poles as well as global coverage with several satellites within the same region.

3.3 Mathematical parameters of the satellite

Once we have obtained the orbits of our constellation, we must be clear about the different angles and parameters of interest for our study. To do so, the following parameters will be calculated, depending on a point on the earth, noted as [lat_{gs},lon_{gs}].

- Elevation angle of the satellite.
- Distance above the ground station.
- Coverage zone.
- Visibility window duration.

The longitudes and latitudes of the different satellites under study will also be required.

3.3.1 Elevation angle of the satellite

For this first parameter it will be necessary to be clear about the geometry we have between the ground station, the satellite point and the centre of the earth. This geometry is described in figure 3.5, obtained in [11]. First, we shall calculate the central angle, a

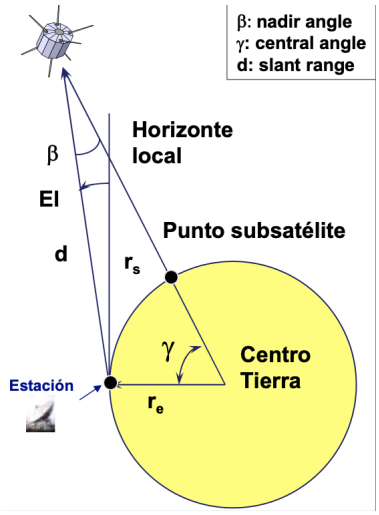

Figure 3.5: Trigonometry of the elevation. [11]

value described by the positions of the earth station and the satellite, referenced in [11].

$$\cos(\gamma) = \cos L_{ae} \cos L_{as} \cos\left(L_{oe} - L_{os}\right) + \sin L_{ac} \sin L_{as} \tag{3.12}$$

where:

- L_{ae}: latitude of the Earth station.
- L_{oe}: longitude of the Earth station.
- L_{as}: latitude of the sub-satellite point.
- L_{os}: longitude of the sub-satellite point.

This angle will give us the ability to obtain the height (h) at which we have our satellite. This parameter can also be extracted from the rotational coordinates, because we can obtain the longitude, latitude and height easily.

Once these variables are characterized, we can easily obtain the elevation angle of our satellite with the equation 3.13, described in [11].

$$\cos El = \frac{\sin \gamma}{\sqrt{1 + \left(\frac{r_e}{r_s}\right)^2 - 2\frac{r_e}{r_s}\cos \gamma}} \tag{3.13}$$

Where:

- r_s: distance from Earth to satellite.
- r_e: Earth radius.
- γ: central angle.

3.3.2 Distance above the ground station

As we have seen in the previous section, one of the most important points to obtain the elevation of our satellite is the height at which it is located. In order to calculate this height, we can look at the equation 3.14 described in [10], with which we will be able to obtain the height at which the satellite orbits.

$$d = r_s\sqrt{1 + \left(\frac{r_e}{r_s}\right)^2 - 2\frac{r_e}{r_s}\cos \gamma} \tag{3.14}$$

In figure 3.6, we can see that it is really a LEO constellation, because we have at all times the satellites at about 500 kilometres above the ground station. We can also validate one of the initial characteristics of the constellation, where in a first launch, the constellation is located above 550 kilometres. It should also be noted that there are several satellites, those that have been launched more recently, given that they have the highest satellite value, which are above 300-350 kilometres given their dependence on solar activity. [17]

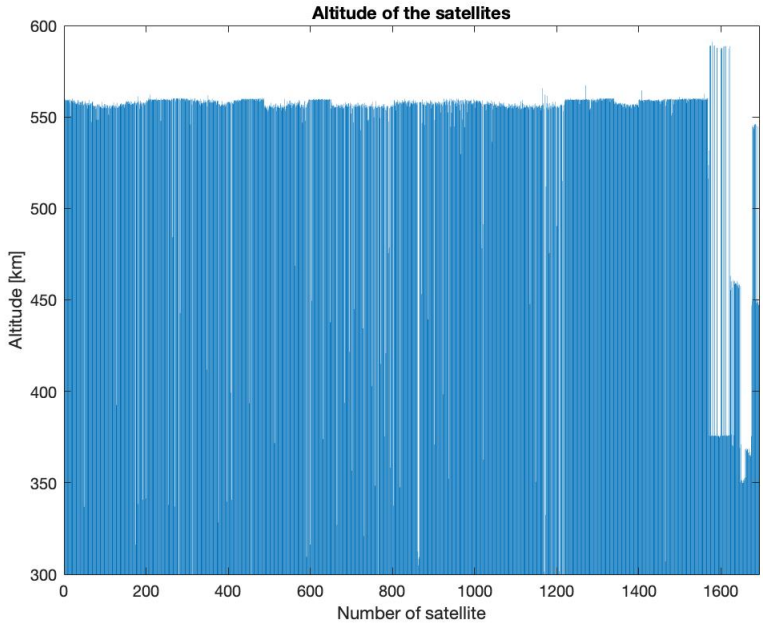

Figure 3.6: Altitude of the satellites.

3.3.3 Coverage zone

For the study of this work, it is necessary to know which of the satellites within the constellation are in coverage with our ground point, because the communication link parameters would not be consistent for elements that are not in view of our study point. Therefore, the coverage parameter will be essential in this study.

Coverage is defined by the following equation, being exposed in [18]:

$$\text{coverage} \ = [\max(-90, -i - \gamma_c), \min(90, i + \gamma_c)] \tag{3.15}$$

As we can see, it has to do with the inclination of our satellite (parameter described in the TLE file) and γ_c, being the central angle, when the elevation is minimum. In the equation 3.16, we can denote as θ_c the minimum elevation angle of the satellite, not the minimum for the user terminal as set out in [19], with a value of 40°.

$$\gamma_c = \text{acos}\left(\frac{re}{r}\cos\theta_c\right) - \theta_c \tag{3.16}$$

Therefore, any satellite within the constellation that is not in coverage with our ground point, we will not be able to interact with it. Once we have obtained the satellites in view of the total constellation from a point on the earth, we can proceed to obtain the visibility time of the satellite, in order to conclude which time window, we can have communication

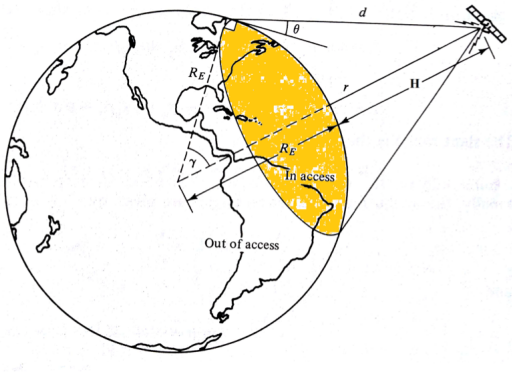

Figure 3.7: Coverage zone of a satellite at altitude H. [13]

with the satellite in question.

3.3.3.1 Visibility window duration

The total visibility time of a satellite is defined as the time interval, of a satellite in coverage, that we are able to see it and therefore have a communication link over it.

For the calculation of this parameter, described in figure 3.8, we will need the following initial data:

- Orbital parameters:
  - Inclination.
  - Minimum elevation.
  - Longitude of ascending node (Ω).
- Ground station position (lat_{gs},lon_{gs}).

Since we have the initial parameters, we are going to obtain the previous calculus in order to obtain the initial variables additionally to the data previously commented. Those parameters are described in the equations 3.17a and 3.17b, exposed in [11].

$$lat_{pole} = 90 - i \tag{3.17a}$$

$$long_{pole} = L_{node} - 90 \tag{3.17b}$$

Bearing in mind that we are working with the real orbits of the satellites of the constellation, it will be relevant to take into account the minimum and maximum longitudes that we move; depending on the minimum elevation angle that they have the satellite.

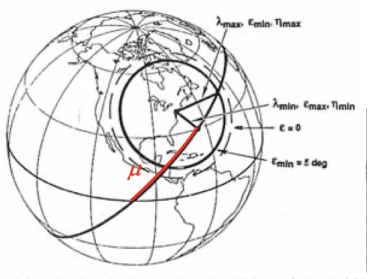

Figure 3.8: Outline of visibility window. [10]

One of the approximations used, considering that the orbit is circular, is defined in the expression 3.18. This approximation will give some certainty in the actual time measurement.

$$\sin \mu = \frac{\sin lat_{gs}}{\sin i} \tag{3.18}$$

In our study, taking into account the trigonometry of our system, and the characteristics of our orbit, we will have to calculate the minimum and maximum longitude at which we will see our satellite. For this we will need the equations described in 3.19a and 3.19b.

$$\sin \lambda_{\min} = \sin \text{ lat }_{pole} \sin lat_{gs} + \cos lat_{pole} \cos lat_{gs} \cos \left(long_{gs} - long_{pole}\right) \tag{3.19a}$$

$$\lambda_{\max} = 90^{\circ} - \varepsilon_{\min} - \eta_{\max} \tag{3.19b}$$

Where:

$$\eta_{\max} = \arcsin(\sin \rho \cos \varepsilon_{\min}) \tag{3.20}$$

Once these values have been calculated, we can relate them to the orbital period retrieved from the TLE file. The visibility time of our satellites are described in 3.21, exposed in [11].

$$T_v = \left(\frac{P}{180}\right) \cos^{-1}\left(\frac{\cos \lambda_{\max}}{\cos \lambda_{\min}}\right) \tag{3.21}$$

Considering that this time is equally distributed from the maximum elevation of each of the satellites, we will be able to recover the vector within visibility of the orbits described in the section 3.3.3.

Once the visibility times of each satellite have been observed, we retrieve the orbit vector within this time space, making the relation between the total samples of our vectors, the total period and the visibility time calculated above.

3.3.4 Parameters of the channel

In this section we will explain and show how we have come to calculate the channel capacity, one of the objectives in order to be able to observe how fast and efficient the Starlink constellation is. To do so, we will review the Shannon capacity at a theoretical level and then apply it with the values discussed in the previous section.

3.3.4.1 Theorem of Shannon-Hartley

Within the transmission process of a telecommunications system, we have noise signals that contaminate the information to be sent. These signals are present everywhere, having different forms of generation as natural phenomena or properly created by elements within the system.

For this, there is the Shannon-Hartley theorem that establishes the maximum capacity of a link according to the bandwidth (B) and the signal-to-noise ratio (SNR); as shown in the equation 3.22.

$$C = B \log\left(1 + \frac{S}{N}\right) \tag{3.22}$$

Where C is the information capacity of the channel, in other words, the maximum bits we are able to send per second along the channel. This parameter is measured in bits per second.

For this study, we will have to take into account that we have two communication links:

- Uplink: ground station - satellite.
- Downlink: satellite - ground station

These two systems will be studied independently, using the data described in [19]. It should be noted that we carried out the study of the capacity in Mbits/s, given the high amount of information that can be sent, it is easier to handle.

Chapter 4

Starlink Constelation

As we have seen in chapter 3, the mathematical model that we will have on stage for our study of the constellation has been discussed.

Once the different expressions have been discussed, this chapter will look at the basic characteristics of the constellation under study, the Starlink constellation. A study will also be made according to the different variables described in the system, such as the position of the ground station or the elevation of the satellite.

This chapter will be essential to be able to observe the main characteristics of the constellation and to be able to draw first empirical conclusions by pushing the boundaries of the constellation.

4.1 Number of satellites

In the previous chapter, we were able to observe, in the figure 3.4, a certain number of satellites in orbit. According to the TLE obtained in [21], we have been able to collect information on 1693 satellites in orbit. These satellites have the orbits described in the figure 4.1.

Given this isometric view of the orbits, we can observe the large number of satellites we have in the central areas of the planet, compared to the minimal appearance of satellites at the poles. In the figure 4.2, modifying the view of the figure 4.1, taking the XY plane, we can confirm this same statement.

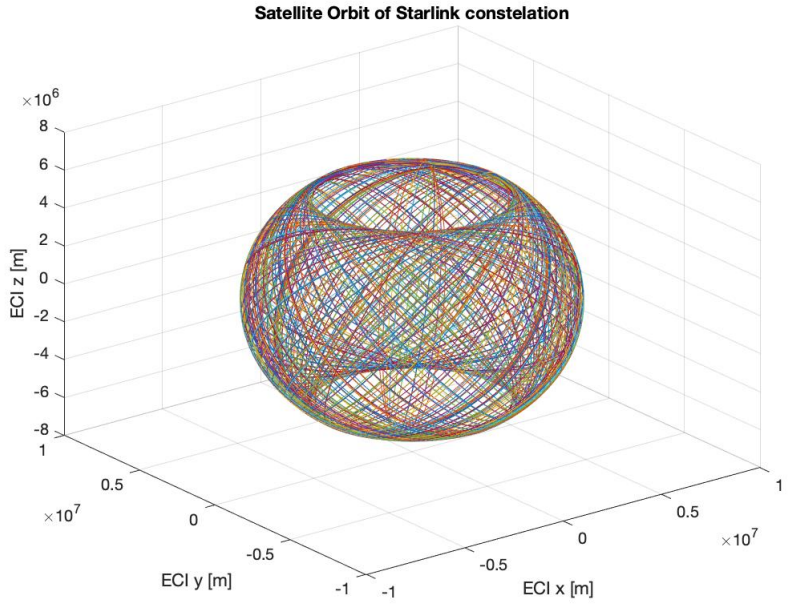

Figure 4.1: Starlink constellation.

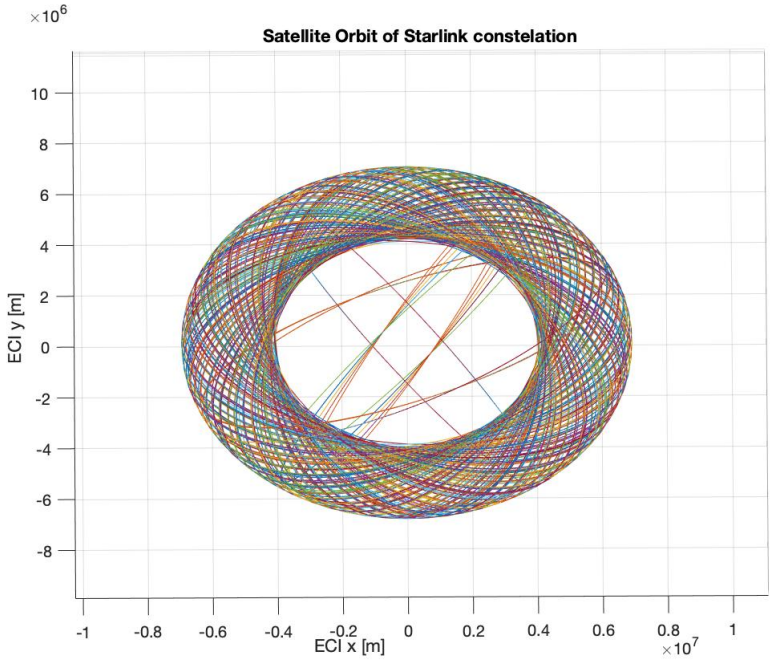

Figure 4.2: Starlink constellation in plane XY.

Continuing in the same vein, the satellites in view will be shown below according to different points on the planet, chosen according to their climate, described in the figure 4.3. This figure, obtained in [27], shows the climate on 25 December 2021.

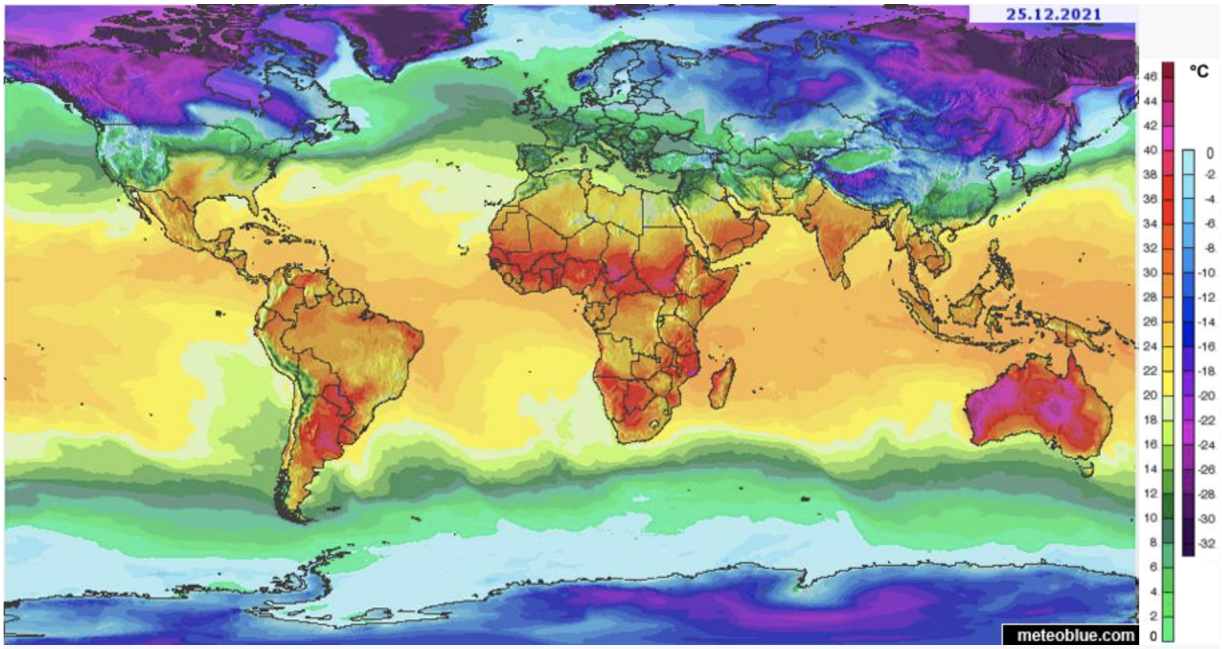

Figure 4.3: Global temperature. [27]

As we can observe, depending on the longitude of our position of the earth station, we will have a more humid and warm climate, or cold and dry. Therefore, taking into account what kind of climate we have, although for now it will be transparent for our study, we will choose the following points described in the following table:

City	Longitude	Latitude
Barcelona (Spain)	2.16992	41.3879
Sao Paulo (Brasil)	-46.6388	-23.5489
Moscow (Russia)	37.6172	55.7508

Table 4.1: Positions under study.

Then, as we can see in figure 4.4, we have a different number of satellites in view. In particular, each city has the following number of satellites in view:

- Barcelona: 1225 satellites.
- Sao Paulo: 1194 satellites.
- Moscow: 1035 satellites.

Bearing in mind that the variation in climate is largely to do with the longitude of the study point. As these values approach the poles, where we have seen that we will have a reduced number of satellites in view, in figure 4.1, we have a considerable reduction. Note

that Barcelona, being the point with the lowest longitude of the three targets. In figure 4.4, we can observe the orbits of the satellites that are capable of obtaining communication with the different points of interest discussed above. Although the variation between the three cities is relatively small, we can observe a variation in the opacity of the spheres, caused by the difference in the total number of satellites with which we obtain vision, and therefore, which are in coverage. These results have been calculated from the explanation described in section 3.3.3. For this, the central angle, described in the equation 3.16, of each of the satellites in the constellation has been calculated and then the coverage margins, described in 3.15, have been obtained.

On the other hand, we can observe that in Moscow, in (b), where we can observe the lowest number of satellites, we have more than 60% of the total in view, taking into account the total satellites described in [21].

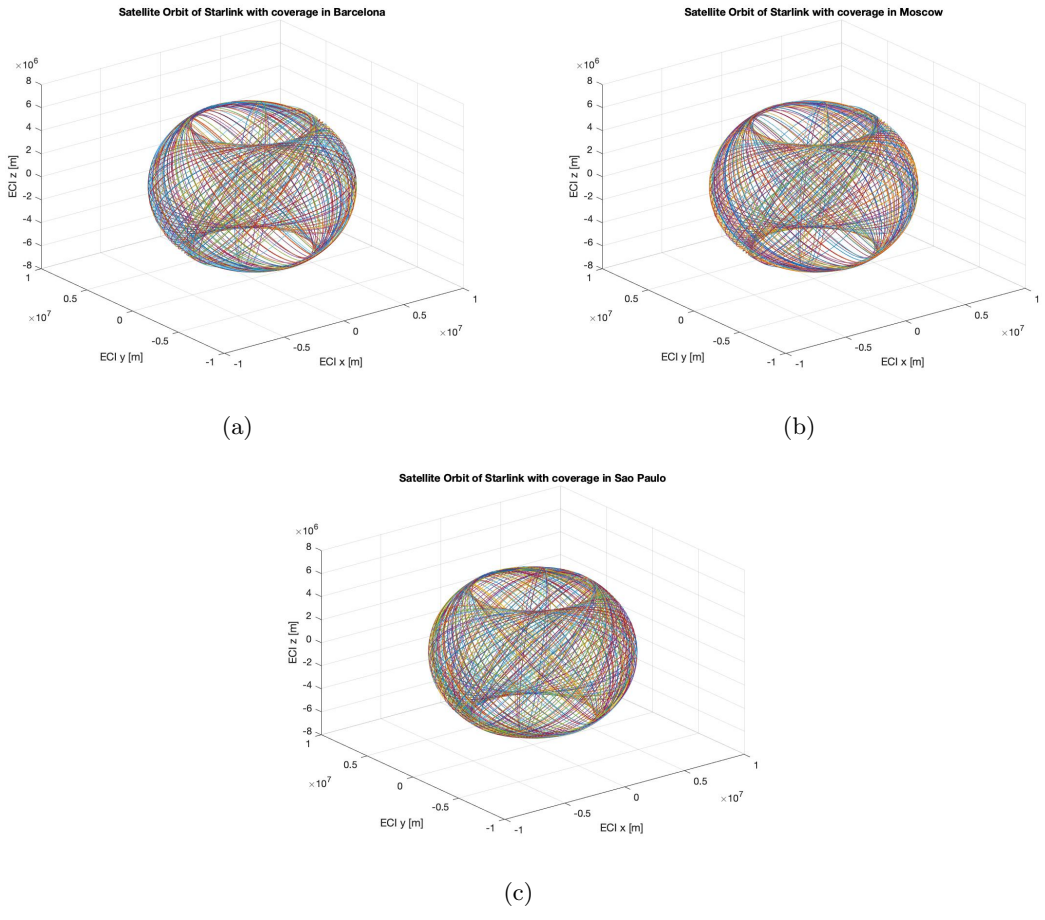

(a) (b)

(c)

Figure 4.4: Number of satellites visibles.

As we have discussed in previous sections, one of the purposes of the Starlink constellation is to provide global population coverage. Looking at the figure 4.5, we can see that we

have many of the satellites concentrated in the most densely populated areas of the world. In the figure, we can see how in the central longitudes, near the equator, we have most of the world's population.

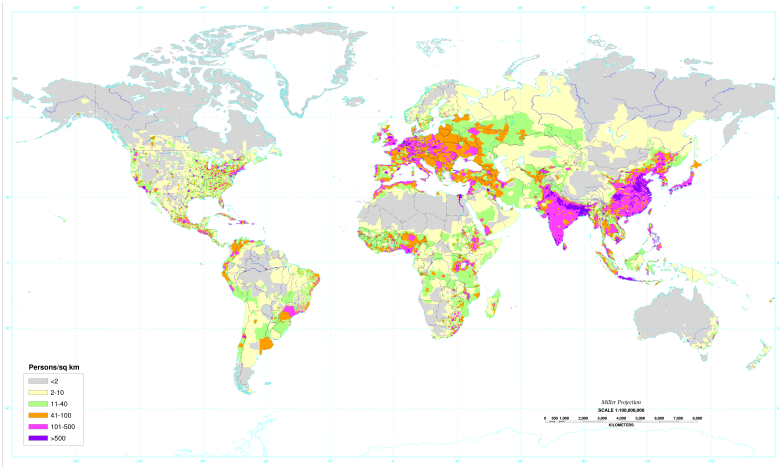

Figure 4.5: Density population of the world. [14]

This statement can be corroborated by looking at the ground track of the satellites in figure 4.6, although we are not able to observe the traces individually, given the high number of satellites in orbit. The accumulation of lines within the central longitudes gives us the necessary information to be able to corroborate one of the objectives of this constellation.

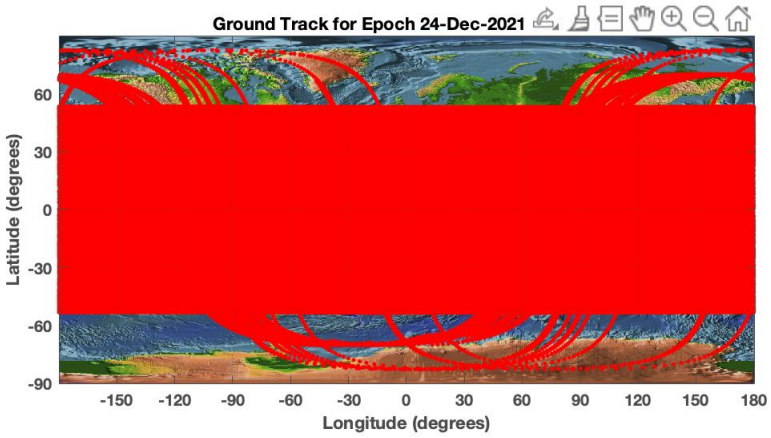

Figure 4.6: Ground track of the Starlink constellation.

4.1.1 Variation in the longitude

In this section we are going to modify the longitude, without taking into account any particular point in the world, so that we can observe how the number of satellites in view changes as we modify this parameter. For this study, we will have a constant latitude, above the equator, so as not to be influenced by this coordinate.

Considering this study scenario, we can observe in figure 4.7, the variability of the number of visible satellites with a constant variation of 1°:

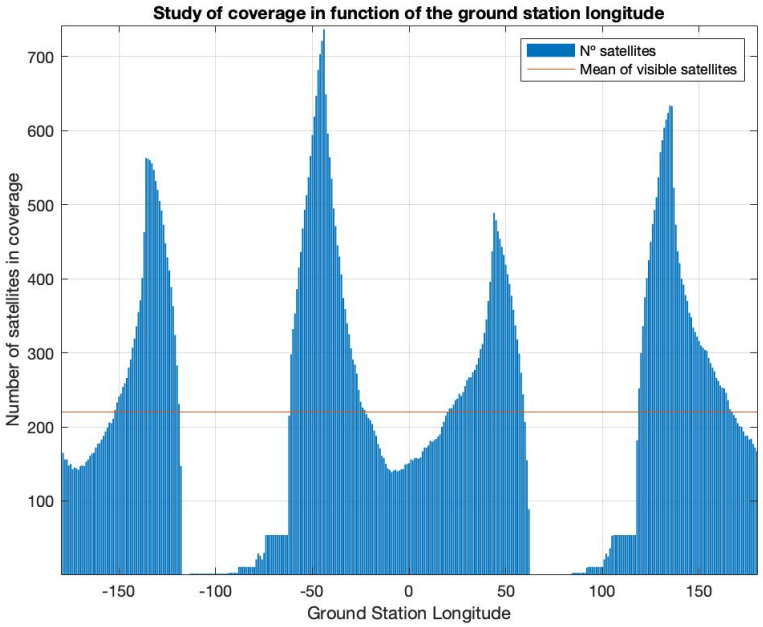

Figure 4.7: Longitude variation.

One of the first considerations we can draw from this variation, correlating with the figures 4.7 and 4.6, is that we have a number of visible satellites within the longitudes where the world's major technological powers are located. We use a latitude equal to 0 grades, in order to not affect to the computation.

Within the figure 4.7, we can observe 4 large peaks where we have many satellites in view. These lengths resemble the values for the United States of America, Asia and Europe. Although Europe has the most satellites, it does not have a variation of more than a hundred satellites.

Another important point to note is the low visibility in the Atlantic Ocean, a curious fact, given that there is not much population density in this region of the world.

4.1.2 Variation in the latitude

At this point, we will modify the latitude value of our ground station in order to observe the variability of the total number of visible satellites. To do this, we will use the code shown above, with the following modifications to the input variables:

```
phi_gs = -90:1:90;
lambda_gs = 0;
```

Note that the longitude in this case falls on the Greenwich meridian, where we have a longitude of 0 degrees. As in section 4.1.1, we show the variation for a central value of planet Earth, minimizing the effect it may have.

As can be seen in figure 4.8, we have a very even visual arrangement at all points on the planet, with an average of 263 visible satellites (approximately 15 percent of the total).

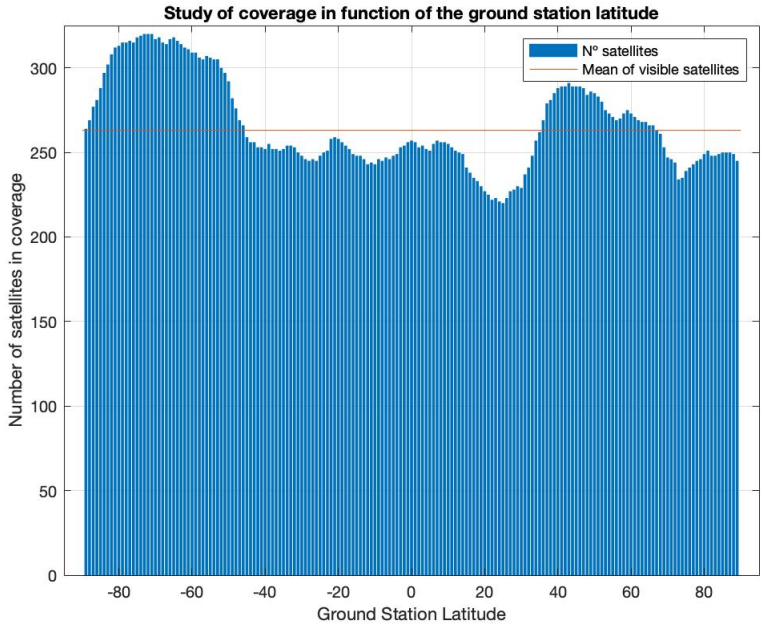

Figure 4.8: Latitude variation.

Since we have a relatively low variation as a function of latitude, we should note that correlating with the figure 4.1, we have most of the satellites within the central latitudes of the planet, leaving the poles uncovered (for now). Emphasising the extremes of the figure 4.8, we can see that at values close to [-90,90], we have no visible satellites at all.

In parallel, looking in detail at the figure 4.2, we see that we have some satellites orbiting above the poles; these do not have sufficient minimum altitude to be seen by a supposed ground viewing station. Therefore, we can further validate the characteristic of this constellation.

4.1.3 Variation in the latitude and longitude

In order to close this study, we will carry out the study of the visibility of the satellites with a double variation. For this purpose, we will make the following modifications to the input parameters of our code described above:

```
phi_gs = -90:5:90;
lambda_gs = -180:10:180;
```

In this case, we will have fewer path points in latitude (phi_{gs}) because the academic version of Matlab is not able to process such a magnitude of data; bearing in mind that we will follow such a study with the whole set of satellites of the constellation [21].

First of all, in figure 4.10, we must explain how the data are being displayed for this part of the study. In this figure, we have on the Y-axes, the total number of satellites we have in view for the points described on the X-axis. On this axis, we have described different sets of bars corresponding to the variation of latitude, within that longitude value.

In order to clarify this explanation, a zoom of the figure 4.10 is added, being the figure 4.9. We can observe different groups of columns, which are about each latitude value, within each global longitude value. Thus, we can observe the variation of the visible satellites, within each longitude; going through all the latitude values of the planet.

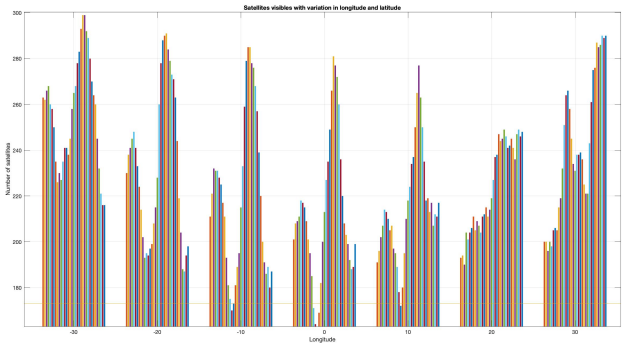

Figure 4.9: Zoom of the figure 4.10

Taking into account the previous explanation, we can observe in figure 4.10 a variation

similar to the one seen in figure 4.7, having the same positional characteristics for the longitudes with more and less appearance of satellites in view. Although this similarity is quite high, we can observe a transversal line within the figure, which marks the average number of satellites in view within all the positions described in this part of the study. In this case, we have approximately half as many satellites in view on average, with the involvement of low visibility latitudes being the main reason for this variation.

Next, we can see that we have the same gaps in view as in figure 4.7, mainly at the positions of the planet's large oceans; as well as the same peaks of coverage within the most densely populated areas. Looking at the differences between the longitude groups, we can see a small difference, because we have the extremes of the latitude values ([90,-90]), with no coverage of any kind. Furthermore, we can observe that the general shape of the coverage shows also within each of the discrete longitudes. That is, we can observe that we have a similar ratio of visible satellites within the different longitudes, making the variation in latitudes.

In conclusion, it is clear that depending on the position of our ground station is crucial to obtain a good number of visible satellites; although this visibility is not homogeneous across the planet. Therefore, this visibility must also be within one of the most densely populated points; otherwise, we will not be able to obtain coverage of any kind or we will have very little time space where we will be able to enjoy it.

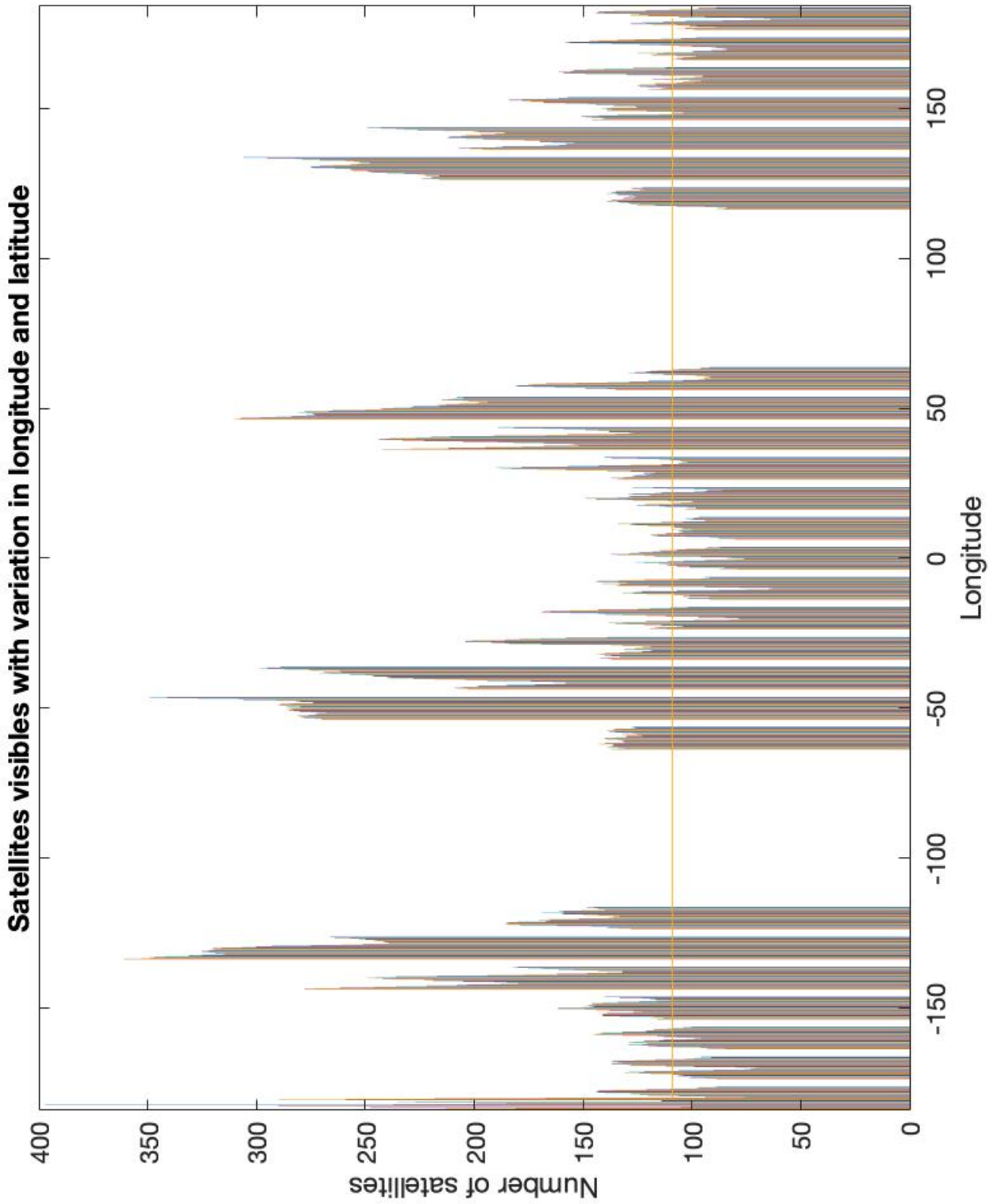

Figure 4.10: Latitude and longitude variation.

4.2 Elevation of the constellation

In this section we will discuss the heights at which we can observe the satellites of the constellation, taking into account all the satellites in orbit, as well as the particular points discussed in the section 4.1. This parameter is essential to know if our satellite is visible by our ground station, because it is one of the factors that makes the central angle of our satellite vary and therefore, it gives us the capacity to observe it or not. In order to obtain the elevation values of the different satellites, we will use the equations described in the section 3.3.1.

4.2.1 Elevation of all the satellites

In this section we propose to obtain the variability of the elevation according to a world point (for this point, Barcelona), observing all the satellites, without taking into account the visibility of the satellites over the ground station.

In the figure 4.11, we can observe the elevation of each of the satellites depending on the selected terrestrial point. This figure is evaluated within a complete orbital period, thus having a total visibility from the initial time point collected from the TLE file, described in 3.1.1.

As can be seen we have many of the points below 0 degrees, this factor shows that the satellites are not visible. In other cases, we have variability in the elevations, obtaining positive values, therefore, with the capacity to be visible but not with the obligatory nature of the same, due to the fact that we also have a relevant factor of the relation between the distance of the satellite and the radius of the earth.

Finally, we can observe in figure 4.11, by analysing the peaks in the figure, that most of the satellites that have a good enough elevation (> 0), are at the beginning or end of the satellite's orbit. In the section 4.2.2, we are going to see the elevations visible for each of the cities of interest. It should be noted that the elevation will not be the only parameter that will have to be computed in order to know which satellites are visible, since the only information that the elevation can give us is when it is a negative value in its entire orbit. In the time lapses that we obtain the positive elevation, it is possible to obtain communication with the satellite, although we must apply the equation 3.15 described in 3.3.3 where we can really know if the satellite under study is visible for our terrestrial position.

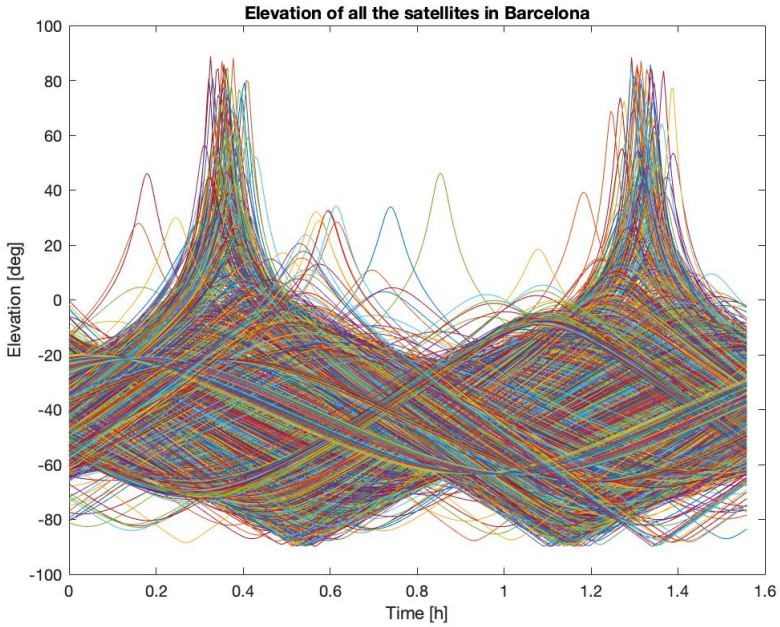

Figure 4.11: Elevation of all the satellites.

4.2.2 Elevation of the visible satellites

In the 3.3.1 section, we have been able to see how we can calculate the elevation of our satellite by using the coordinates of the satellite under study and a particular position for the ground station. For this, the points commented in the table 4.1 are selected, causing a complete study of the planet Earth, focused on the climatic point. In later sections, it will be studied what effect the climate of each of the points has on these communications.

- Barcelona described in the figure 4.12.
- Sao Paulo described in the figure 4.13.
- Moscow described in the figure 4.14.

Noting that these values can give us an initial idea of the number of satellites visible for each of the points (study carried out in the section 4.1), we will also be able to observe another important detail within the characterization of each of the satellites, the visibility time of each of them.

As we can see the elevation, in all cases, has a pyramidal shape because we have a value within the orbit where we start to be able to have communication with the satellite, until we reach the maximum point of elevation; until finally we stop having such communication.

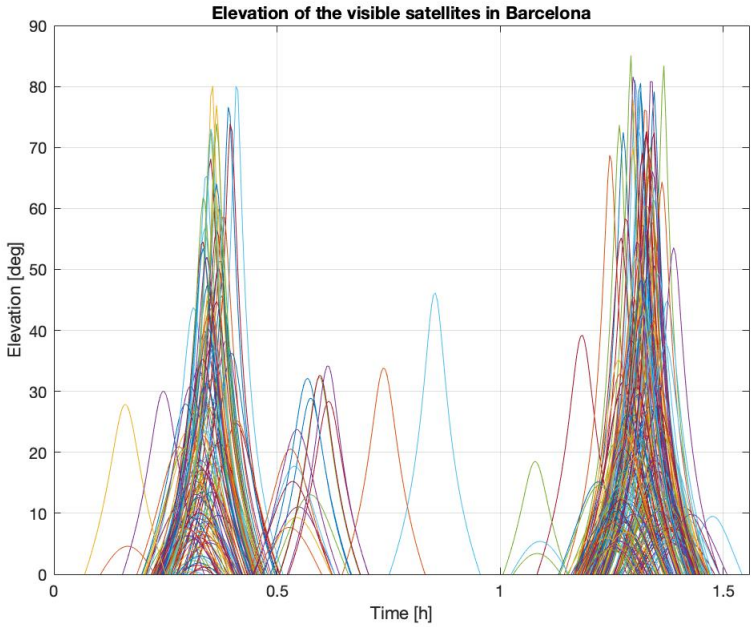

Figure 4.12: Visible elevation of Barcelona.

This behavior, taken to the elevation we describe as all values above zero degrees, with a maximum. The wider this pyramid shape, the longer the communication link with the satellite in question.

Therefore, for good communication, it is not so much the maximum elevation value of the satellites that is essential, but also the time it takes for them to reach their maximum elevation and their subsequent disappearance.

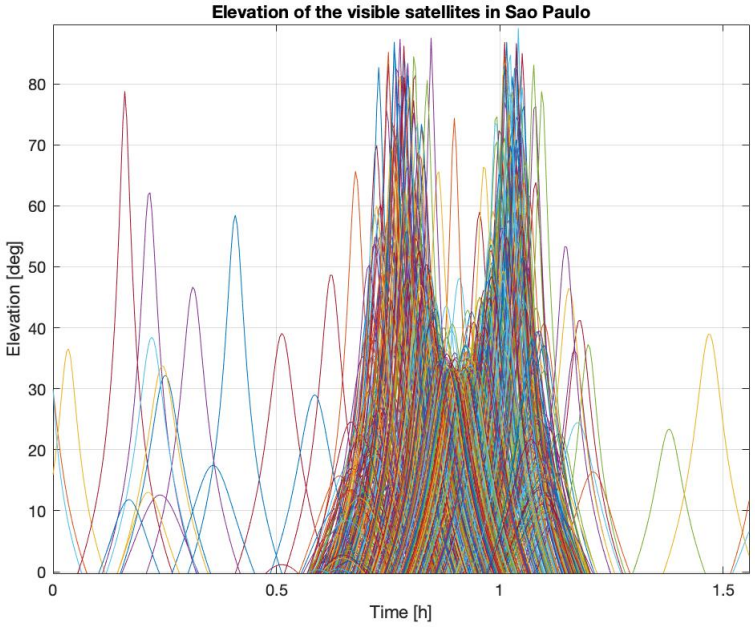

Figure 4.13: Visible elevation of Sao Paulo.

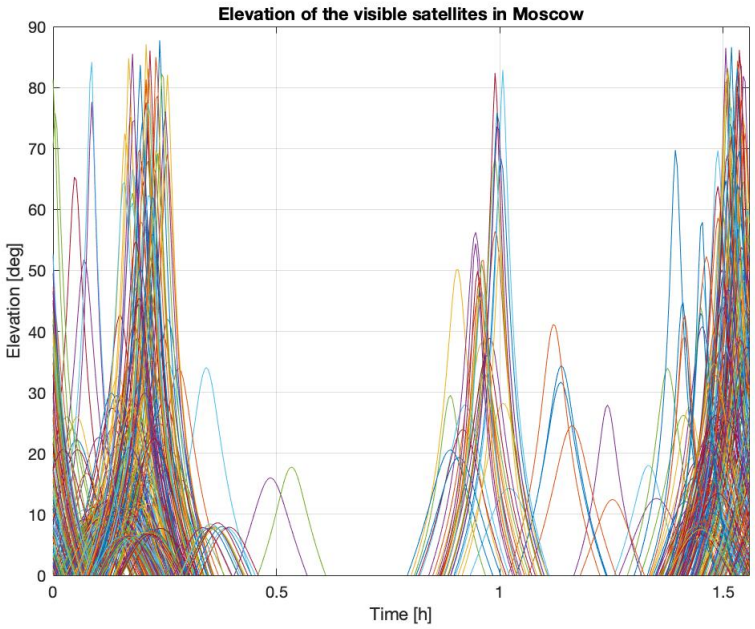

Figure 4.14: Visible elevation of Moscow.

4.3 Time visibility of the satellites

This section will show the visibility time of the satellites we have in coverage within the whole constellation. For this purpose, the expressions discussed in the section 3.3.3.1 will be used, taking into account Barcelona as a first study point to observe this parameter.

As we have seen in the previous section, of all the satellites in the constellation, only the positive elevations, according to the study point, will be the moments where we will have visibility. Therefore, the more time we have positive elevation, the more time we will have communication with the satellite in question.

In figure 4.15, we have represented the visibility time (in hours), for each of the satellites, having a minimum visibility time of approximately 70 minutes. In this graph, referenced on the X axis for each of the 1693 satellites [21], it can be observed that some of the satellites have a time equal to 0; this is due to the fact that this satellite has no coverage for our earth station point, caused by the fact that it has no time of vision given the relationship between the satellite position and the terrestrial position. In order to be able to observe which satellites we have the capacity to observe, and therefore, to know what the visibility window of the satellite is, we have worked with the coverage described in the section 3.3.3 and the expression of the visibility time described in 3.3.3.1. It should also be noted that the study window is based on the day of data extraction from the TLE file [21] and on a time span equal to one day as well.

Note that the first 800 satellites in the constellation have similar coverage to the study point, as opposed to the last satellites launched, since few of them have visibility. Next, as in previous sections, we will consider the other two points of interest of the study.

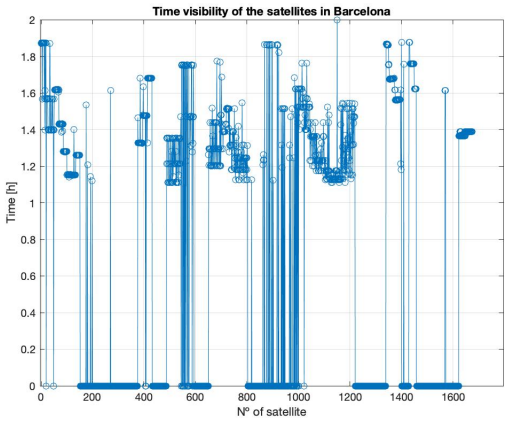

Figure 4.15: Time visibility of the satellites in Barcelona.

To this end, the figures 4.16 and 4.17 are added, where we can observe the visibility time of the satellites.

Particularly for the figure 4.16, we can observe that the number of satellites in view, i.e. with a time greater than 0 minutes, is reduced compared to Barcelona, described in the figure 4.15. We can also comment that the average visibility time is somewhat shorter; therefore, we can conclude that in Moscow we will have worse conditions for communication with the constellation.

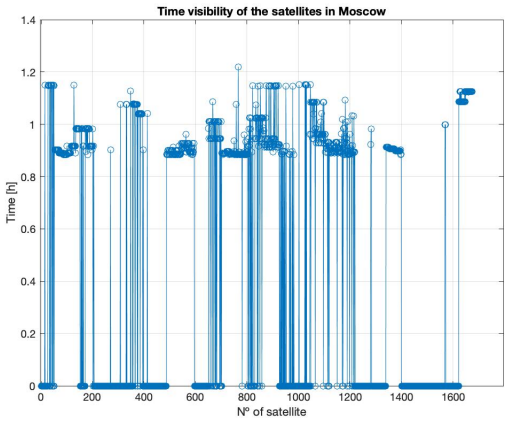

Figure 4.16: Time visibility of the satellites in Moscow.

Finally, in figure 4.17, we show the visibility time of the satellites in coverage for Sao Paulo. As we can see, this is the location where we observe the least variance within the values obtained. In terms of number of satellites, we can see that we have a value similar to that of Barcelona, but somewhat smaller, as we can see in the previous figure 4.4.

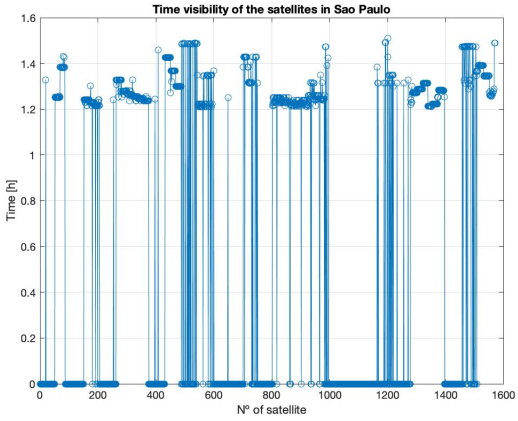

Figure 4.17: Time visibility of the satellites in Sao Paulo.

4.3.1 Study of the time visibility

Once we have been able to observe the times for discrete points on our planet, the variation of the same time will be shown, taking into account a variation of longitude and latitude. In this variation, we will have an idea of how it affects the visibility time depending on the position of our earth station.

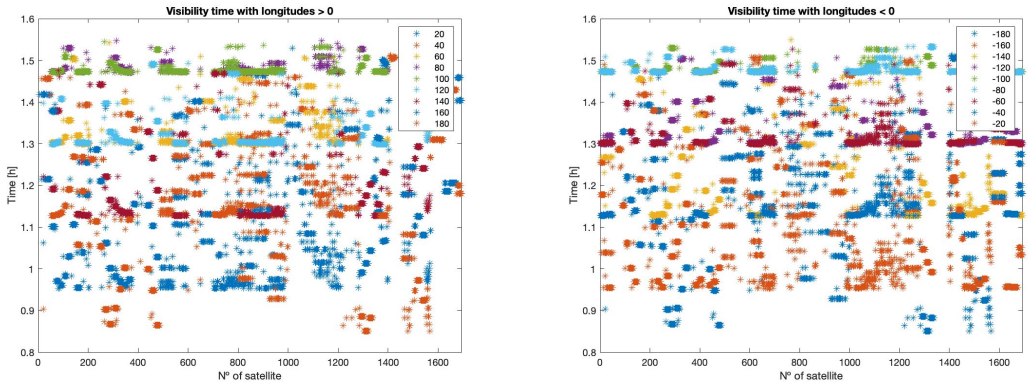

(a) (b)

Figure 4.18: Variation in longitude on the time visibility.

In figure 4.18, we can observe two variations by longitude; in (a), a variation for lengths greater than 0 degrees; in (b) a variation for negative longitudes. In this figure, we obtain the visibility time of each of the satellites in the constellation in order to obtain the differences that the same satellite may have at different latitudes and/or longitudes.

First of all, it is necessary to note that the data for each of the longitudes, at the level of available satellites, are not the same, therefore, we will not always be able to observe the visibility time of one of the satellites for all longitudes.

One of the factors that we can easily observe is that we have a downward variation of the visibility time when we are at the extremes of the longitudes; however, this variation is in decimal parts of an hour; therefore, not very influential.

Next, in figure 4.19, we can observe the same version of variation, but this time by the latitude of the earth station position.

By zooming in on a series of satellites, we can easily observe the behavior of the same satellite, taking into account the variation of latitude. This behavior can be seen in the figure 4.20. In it we can see that the visibility time of this set of satellites improves as the latitude increases; therefore, when we are in the northern hemisphere of the planet, we

have greater availability of coverage with the satellites than in the southern hemisphere. Although the variability of this parameter is not crucial for communication between the base station and the satellite, since we are talking about a lower variation , we continue to see a trend towards greater performance in areas where we have a higher population density and, in turn, greater purchasing power.

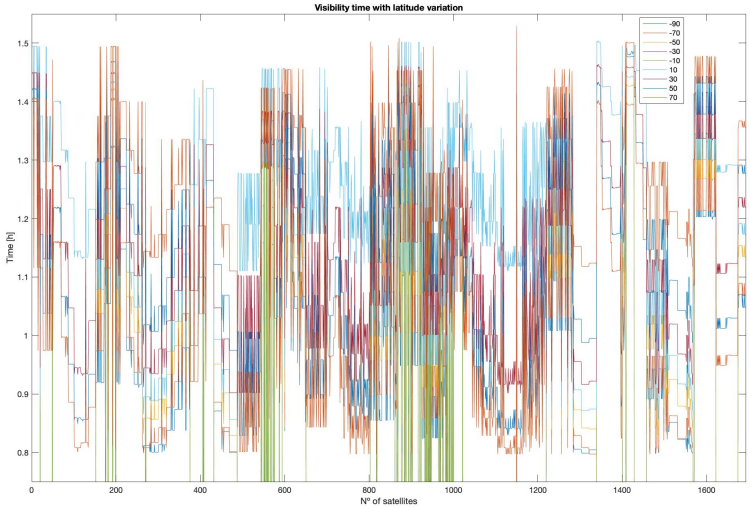

Figure 4.19: Variation in latitude on the time visibility.

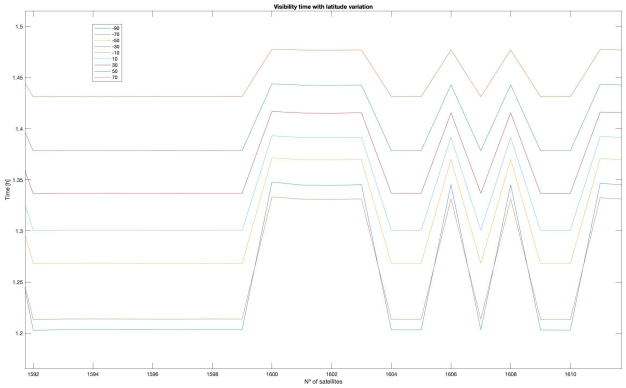

Figure 4.20: Zoom of figure 4.19.

Chapter 5

Capacity of the channel

5.1 Channel models

This chapter will show what our channel model is, taking into account all the described losses within our radio link. To do so, we will refer to the ITU recommendations where the different attenuations based on atmospheric phenomena are explained. The value of the useful signal of our system will also be discussed.

5.1.1 Effects on signal propagation

As we have seen in section 3.3.4.1, the channel capacity is described by the ratio between the useful signal and the noise signal. In order to study this parameter, it is essential to know the total power captured by the system, taking into account different losses due to different reasons, such as environmental or system losses.

To calculate these powers, we must consider the power balance of the system. To do this, we will take into account different parameters, described in 5.1 and 5.4.

$$S = EIRP - FPSL - L_{atm} + G_{rx} \tag{5.1}$$

Where:

– Effective Isotropic Radiated Power (EIRP): output power of a signal when it is concentrated into a smaller area by the antenna. This parameter include the losses of the cable that connect de transmitter with the antena and, included also de antenna gain.

$$EIRP = P_{TX} - L_C + G_a \tag{5.2}$$

- Free-space path loss (FSPL): attenuation of radio energy between the feed points of two antennas that results from the combination of the receiving antenna's capture area plus the obstacle-free, line-of-sight path through free space.

$$FSPL = \left(\frac{\lambda}{4\pi d}\right)^2 \tag{5.3}$$

- Atmospheric losses (L_{atm}): is the sum of all climate-related losses at our study point on land. For this purpose, the following losses have been considered, related to the corresponding ITU.
  - Cloud attenuation: related with ITU-R P.840-6.
  - Gas attenuation: related with ITU-R P.676-12.
  - Rain attenuation: related with ITU-R P.618-13.

  The sum of these independent attenuations gives the total attenuation due to atmospheric phenomena.
- Gain of the receiver antenna (G_{rx}).

Another relevant point of our system will be the total noise power. For this we will use the equation described in 5.4. In it, we will take into account the operating bandwidth of our system (being different for uplink and downlink) and the temperature at which the system works.

$$N = kTB \tag{5.4}$$

Once the signal and noise powers have been calculated, we can obtain the signal-to-noise ratio (SNR), described in 5.5.

$$SNR[dB] = S - N \tag{5.5}$$

5.1.2 Rain attenuation

As we have seen in the previous section, we will take into account different attenuations due to the climatic conditions of our terrestrial point under study. First of all, we will take into account the attenuation caused by rain. For this purpose, we will use the explanations described in ITU-R P.618-13.

First of all, we must take into account the scheme described in figure 5.1, where we will have several important points to take into account:

- h_r: rainfall height given in [33].
- h_s: height above sea level of the ground station.
- θ: antenna elevation, being a minimum of 40 degrees.

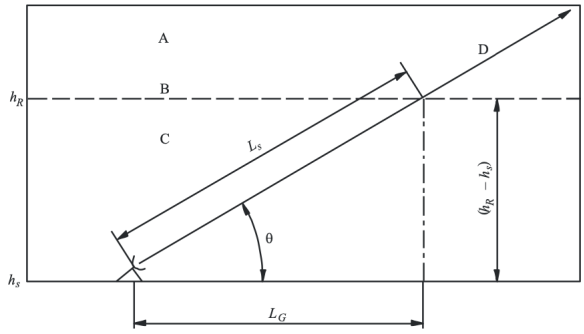

Figure 5.1: Schematic representation for the parameters. [30]

Next, taking into account that the minimum elevation will be 40 degrees, we will have to calculate the length of the oblique path (L_s), with the equation described in 5.7b. In case the elevation of our antenna is less than 5 degrees, we would have to proceed with a somewhat more complex equation described in 5.6.

$$L_s = \frac{2\,(h_R - h_s)}{\left(\operatorname{sen}^2\theta + \frac{2(h_R - h_s)}{R_e}\right)^{1/2} + \operatorname{sen}\theta} \tag{5.6}$$

The height above sea level of the ground station position is a known variable and the height of rainfall (h_r), will be obtained by the equation described in 5.7a.

$$h_R = h_0 + 0,36 \text{ km} \tag{5.7a}$$

$$L_s = \frac{(h_R - h_s)}{\operatorname{sen}\theta} \tag{5.7b}$$

Note that if the difference between the heights ($h_r - h_s$) is less than or equal to zero, we will have a rain attenuation equal to zero, regardless of the percentage of time under study (ρ).

Once the values described above have been calculated, we can calculate the last distance described in the figure 5.1, being L_g, the horizontal projection, described in 5.8.

$$L_G = L_s \cos\theta \tag{5.8}$$

For the next step, we will need to calculate the rainfall intensity ($R_{0.01}$), which is exceeded during 0.01% of an average year. These values are taken from ITU-R P.837. This value, when equal to zero, gives us a total attenuation of 0 dB. With this value, we are able to obtain the specific attenuation per kilometre, described in 5.9.

$$\gamma_R = k\,(R_{0,01})^{\alpha} \tag{5.9}$$

Finally, we can obtain the horizontal reduction factors ($r_{0.01}$) and the vertical adjustment factors ($v_{0.01}$), described in 5.10a and 5.10b.

$$r_{0,01} = \frac{1}{1 + 0,78\sqrt{\frac{L_G \gamma_R}{f}} - 0,38\left(1 - \mathrm{e}^{-2L_G}\right)} \tag{5.10a}$$

$$v_{0,01} = \frac{1}{1 + \sqrt{\operatorname{sen}\theta}\left(31\left(1 - \mathrm{e}^{-(\theta/(1+\chi)))}\frac{\sqrt{L_R \gamma_R}}{f^2} - 0,45\right)\right.} \tag{5.10b}$$

With all the previous calculations computed, we can easily observe the rainfall attenuation predicted for 0.01% of an average year:

$$A_{0,01} = \gamma_R L_E \tag{5.11}$$

Where:

$$L_E = L_R \vee_{0,01} \tag{5.12}$$

As we have been able to observe the parameters described in ITU-R P.618-13, they are set by the latitude and longitude of our study point; as well as the study frequency, the percentage over a year and the minimum elevation. For this purpose, the following Matlab function has been created, taking into account the variables described above.

```
att  = rainAttenuation(freq,lat,lon,elev,p);
```

5.1.2.1 Variation in the frequency

First, the variability of attenuation as a function of frequency of use will be studied. Since the satellites of the Starlink constellation are in the Ka (18-31 GHz) and Ku (12-18 GHz) frequency bands.

As we can see in the figure 5.2, we have more losses as the frequency of use increases. Therefore, in the uplink, we will have more losses than in the downlink. Although we have more losses on the frequency side, the increase in frequency gives us the ability to increase the data volume in the radio communication with the satellite.

It should also be noted that the working point for our study is marked in the same figure with * according to the data obtained in [19].

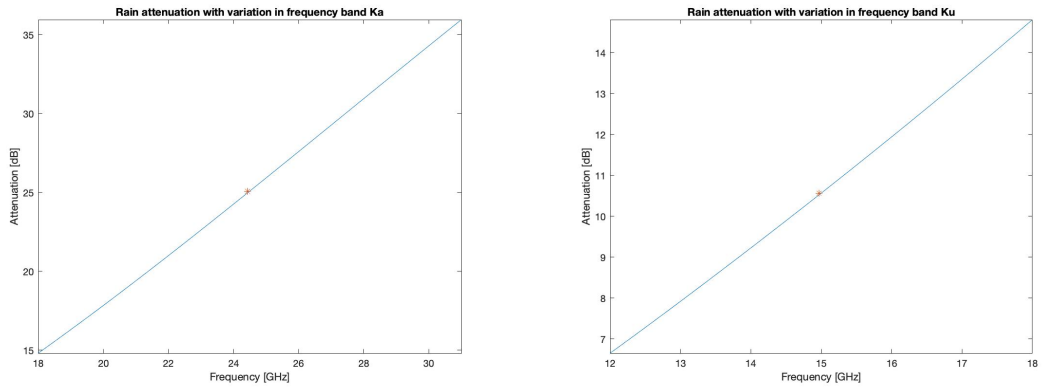

(a) (b)

Figure 5.2: Variation of the rain attenuation in function of frequency bands Ka and Ku.

5.1.2.2 Variation in the percentage of an average year (p)

In this we are going to observe the implication of the percentage of an average year, by changing the value from the typical value (0.01%) to 1.00%.

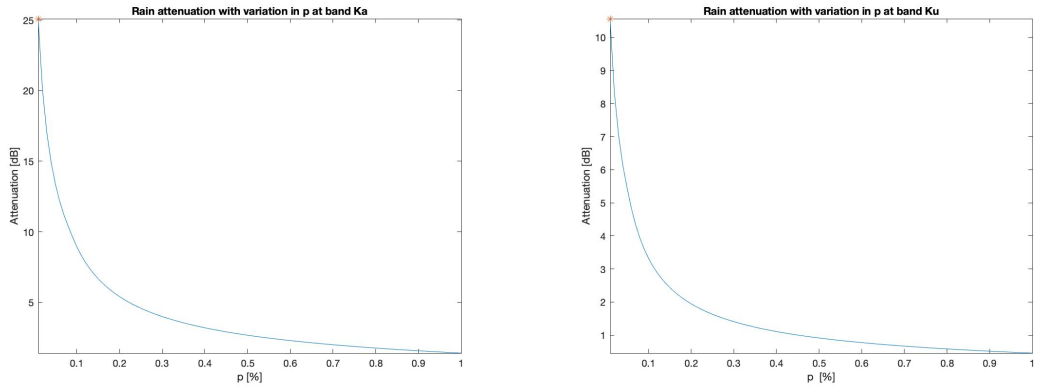

(a) (b)

Figure 5.3: Variation of the rain attenuation in function of percentage at bands Ka and Ku.

In this case, the shape of the graph is given by the rainfall rate ([mm/h]) exceeded for p% of an average year, described in ITU-R P.837-5 and [9]. As we can see in figure 5.4, we have the same condition. As we modify the value of the percentage, keeping the values of latitude and longitude fixed, we observe a decrease in the attenuation. Also note that we see the same behaviour as in the previous point, since we have a higher average attenuation at higher frequencies.

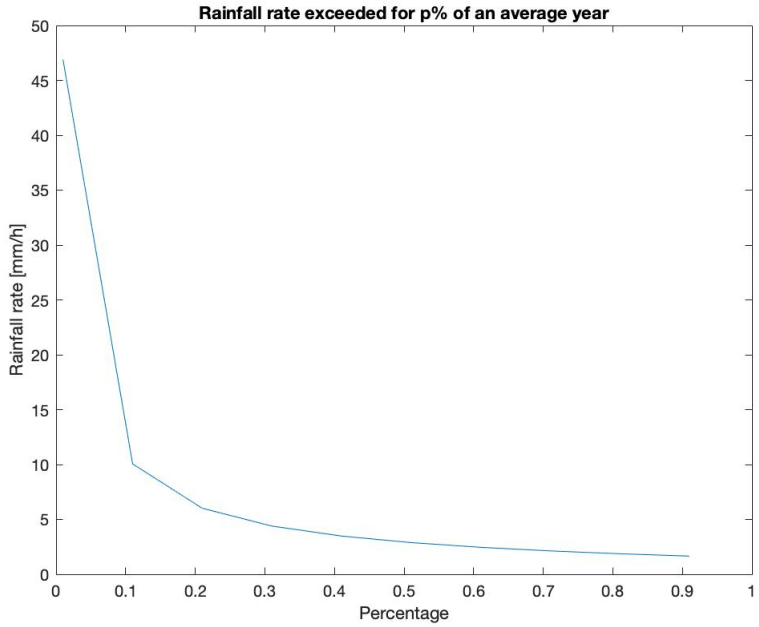

Figure 5.4: Variation of the rainfall.

5.1.2.3 Variation in the longitude and latitude of the ground station

As we have seen in the section 4.1.2 and 4.1.1, where we have varied the latitude and longitude of the ground station to be able to observe the variability of the satellites in view, in this case we will look at how the attenuation caused by rain varies. For this variation study and all subsequent studies, the following two cases will be considered:

Case	Value of longitude	Value of latitude
Variation in longitude	-180º to 180º	0º
Variation in latitude	0º	-90º to 90º

Table 5.1: Value of de variation values.

In the figure 5.5, we can observe a large attenuation at the equator of the earth, with two secondary peaks at 40º and -40º.

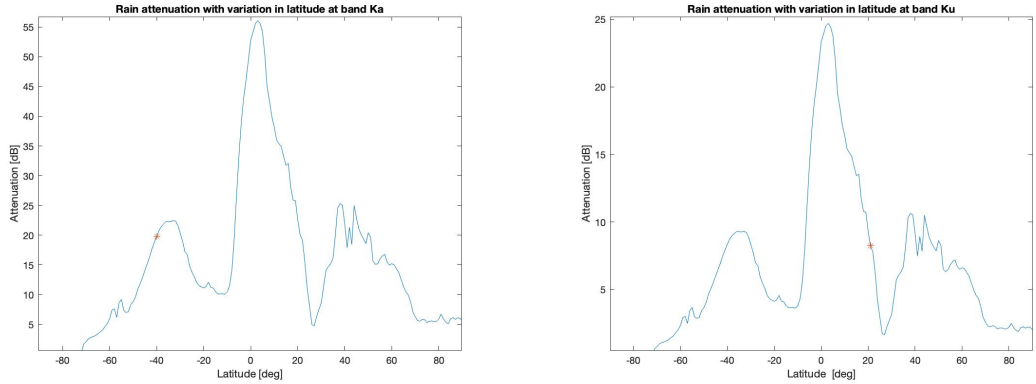

(a) (b)

Figure 5.5: Variation of the rain attenuation in function of latitude at bands Ka and Ku.

Emphasising the peak values, and taking into account the value of the longitude, we observe the peak attenuations in central African areas, where a priori, we should not observe so much attenuation. As we have seen in section 5.1.2, one of the most important factors in the calculation of attenuation is the rainfall rate exceeded for p% of an average year ($R_{0.01}$), described in the equation 5.9. This value can be obtained from the ITU-R PN.837-1, represented in the figure 5.6. We observe that at latitudes close to 0 degrees, we have a greater intensity of rainfall, leading to a very abrupt difference with the areas surrounding this point. Por lo tanto, podemos validar el comportamiento de estas pérdidas en función de la latitud, observando una característica curiosa de las mismas.

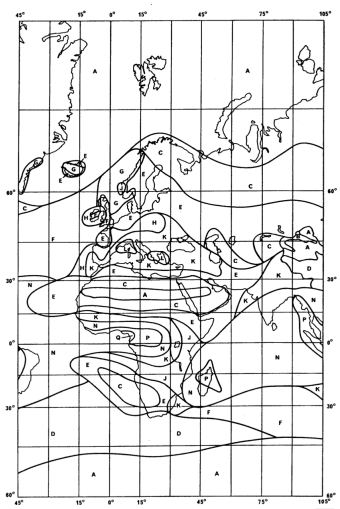

Figure 5.6: Map of the values of rainfall. [32]

The values associated with the letters in the figure 5.6, are described in the figure 5.7.

Percentage of time (%)	A	B	C	D	E	F	G	H	J	K	L	M	N	P	Q
1.0	<0.1	0.5	0.7	2.1	0.6	1.7	3	2	8	15	2	4	5	12	24
0.3	0.8	2	2.8	4.5	2.4	4.5	7	4	13	42	7	11	15	34	49
0.1	2	3	5	8	6	8	12	10	20	12	15	22	35	65	72
0.03	5	6	9	13	12	15	20	18	28	23	33	40	65	105	96
0.01	8	12	15	19	22	28	30	32	35	42	60	63	95	145	115
0.003	14	21	26	29	41	54	45	55	45	70	105	95	140	200	142
0.001	22	32	42	42	70	78	65	83	55	100	150	120	180	250	170

Figure 5.7: Table of the rainfall intensity exceeded (mm/h). [32]

On the longitude side, we can observe that we have a relatively small variation in the Ka-band, because we have a variation of about 3 dB. On the band side, although the variation seems to be the same, as we have more losses, this variation increases. In this case, we have up to 20 dB depending on the position of our station.

The variation in longitude is still described by the same figures of [32], where we can observe that at longitudes such as -60 degrees, being positioned over South America, we have a practically maximum value in rainfall rate; the same happens at longitudes close to 100 degrees, positioned on south Asia, observing the same value.

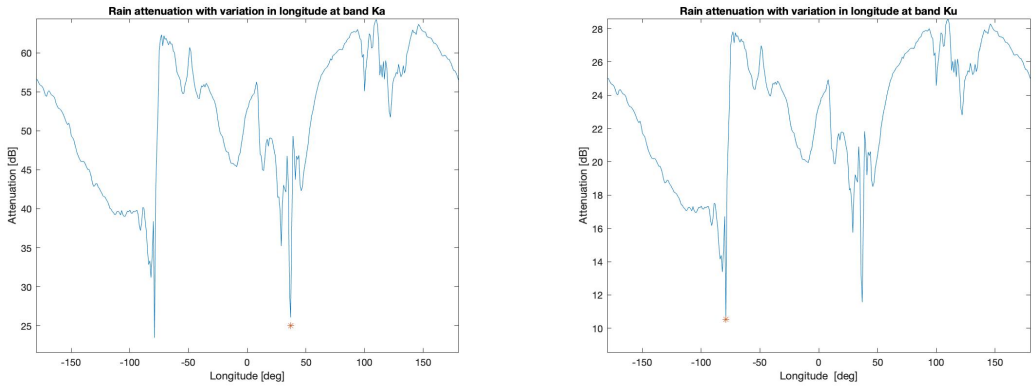

(a) (b)

Figure 5.8: Variation of the rain attenuation in function of longitude at bands Ka and Ku.

5.1.3 Cloud attenuation

Secondly, we enter into the study of the attenuation due to clouds appearing within the communication link. For this purpose, we will use the algorithm described in ITU-R P.840-6 [29].

This algorithm proposes a specific attenuation per kilometre, using the Rayleigh

approximation, valid up to a frequency of 200 GHz. This expression is shown in 5.13.

$$\gamma_c(f,T) = K_l(f,T)M \tag{5.13}$$

Where:

- γ_c: specific attenuation (dB/km) in the cloud.
- K_l: specific attenuation coefficient of cloud liquid water ((dB/km)/(g/m3)).
- M: density of liquid water in the cloud or fog(g/m3).
- f: frequency.
- T: cloud liquid water temperature (K).

We consider clouds and fog to be entirely composed of minute droplets, hence of liquid water. This consideration gives the values for temperature (T = 0°) and water density; typically 0.05 g/m3 and 0.5 g/m3 for thick fog.

Next, taking into account that the value of M is a given value, we will proceed to calculate the specific attenuation coefficient of the liquid water in the cloud, described in 5.14.

$$K_l(f,T) = \frac{0,819f}{\varepsilon''(1+\eta^2)} \tag{5.14}$$

Where:

$$\eta = \frac{2+\varepsilon'}{\varepsilon''} \tag{5.15a}$$

$$\varepsilon''(f) = \frac{f(\varepsilon_0-\varepsilon_1)}{f_p\left[1+(f/f_p)^2\right]} + \frac{f(\varepsilon_1-\varepsilon_2)}{f_s\left[1+(f/f_s)^2\right]} \tag{5.15b}$$

$$\varepsilon'(f) = \left[\frac{\varepsilon_0-\varepsilon_1}{1+(f/f_p)^2}\right]^{+} \left[\frac{\varepsilon_1-\varepsilon_2}{1+(f/f_s)^2}\right]^{+\varepsilon_2} \tag{5.15c}$$

Finally, given the total content of the cloud liquid water column at a temperature of 273.15 K$^{\text{o}}$ (L_{red}), the probability p and the elevation angle, we can obtain the total attenuation, described in 5.16 and obtained in [29].

$$A = \frac{L_{red}K_l(f,273,15)}{\operatorname{sen}\varphi} \tag{5.16}$$

This algorithm is described within the Matlab function below:

```
[ att ] = cloudAttenuation(freq,lat,lon,elev,p)
```

Once the process of obtaining the attenuation by clouds has been obtained, we must undertake a study according to the variable values shown in the Matlab function above.

To do this, we proceed to the same study as above, although without the frequency variation, as it has a linear behavior, giving more losses at higher frequencies; being in our study the Ka band. It should also be noted that at frequencies lower than 100 GHz, we will have an insignificant attenuation within the system [29] .

5.1.3.1 Variation in the percentage of an average year (p)

In this study of the variation of the average percentage of the year (p), we must bear in mind that the values that we will be able to recover according to the probability will be those described in the table below.

Any other value, we will not have values to be able to recover and will cause an error in the calculation. Therefore, we can observe in the figures 5.9 the attenuation as a

	Available values
p [%]	0.1,0.2,0.5,1,2,3,5,10,20,50,60,70,80,90,95,99

Table 5.2: Available values of p.

function of the p-value, observing what was commented previously, seeing that we do not have a large attenuation for this effect.

We can also observe that for certain very high probabilities, there is no information about it; therefore, the total attenuation for this effect disappears. This can be understood because according to the point of study (in this case Barcelona), there is no data for such a high probability of clouds, given its coastal Mediterranean climate.

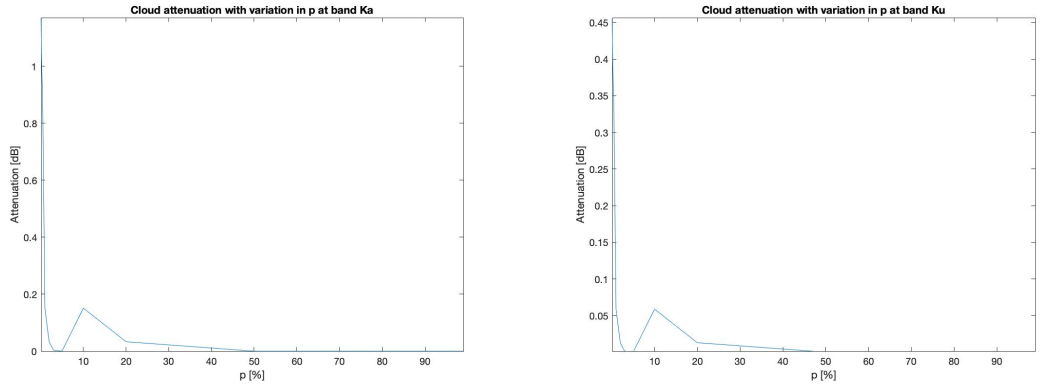

(a) (b)

Figure 5.9: Variation of the cloud attenuation in function of p at bands Ka and Ku.

5.1.3.2 Variation in the longitude and latitude of the ground station

Finally, it will show the variation we have in the attenuation with the modification of the latitude and longitude values of our earth station.

As we can see in the figure 5.10, we have large attenuations above the equator of the earth, just as we have seen in the figure 5.5 in the previous section. Although we have the same shape, we have a much lower value of total attenuation. This behaviour is totally similar to that obtained in figure 5.5, where we observe the variation of the attenuation caused by rain as a function of latitude, this is due to the same precondition. As we have seen in figure 5.6, we have a large rain disturbance, leading in turn to a large occurrence of clouds. As far as the variation in longitude is concerned, in the figure 5.11, we see large

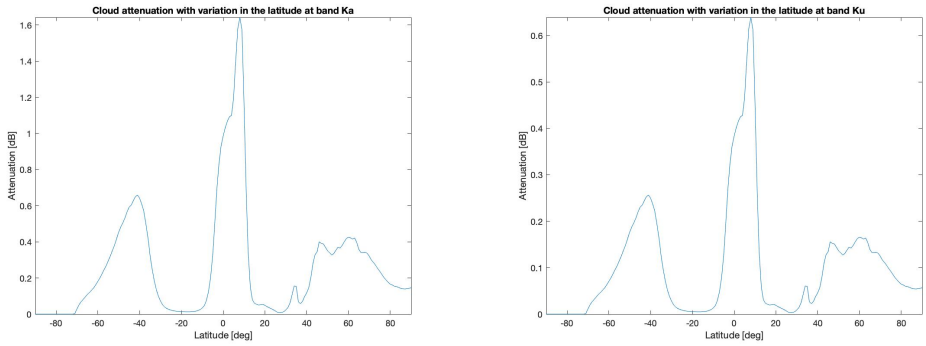

(a) (b)

Figure 5.10: Variation of the cloud attenuation in function of latitude at bands Ka and Ku.

variations depending on our position, although this value is not very appreciable within the system, given again, it is low value. We again observe the same peaks as in the study of the 5.1.2 section, given the same relationship between rain and clouds.

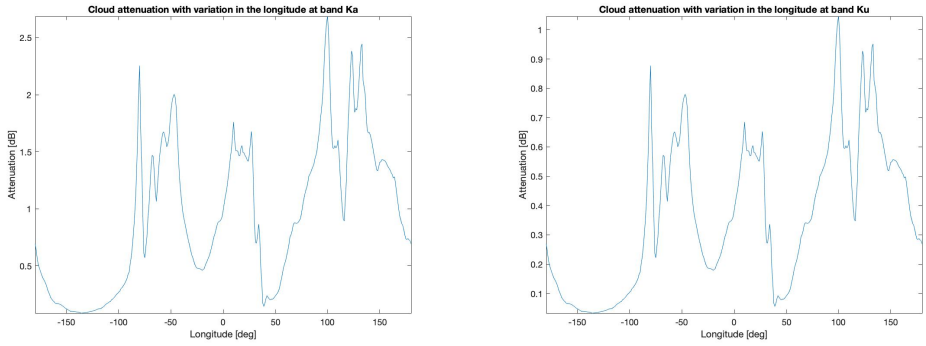

(a) (b)

Figure 5.11: Variation of the cloud attenuation in function of longitude at bands Ka and Ku.

5.1.4 Gas attenuation

The attenuation caused by atmospheric gases, described in [31], presents the estimate of the attenuation caused by gases by summing the individual absorption streaks; within the frequency range of 1 to 350 GHz.

For this purpose, the specific attenuation due to oxygen (γ_o) and the specific attenuation due to water vapor (γ_w) are presented. The sum of these attenuations together with the equivalent height at which they appear (as a function of frequency), will give us the ability to observe the total attenuation values, an expression described in 5.17.

$$A = \frac{A_o + A_w}{\operatorname{sen} \varphi} \tag{5.17}$$

Where:

$$A_o = h_o \gamma_o \tag{5.18a}$$

$$A_w = h_w \gamma_w \tag{5.18b}$$

The specific attenuation values are described in 5.19 and 5.20. Those equations are exposed in [15].

$$\gamma_o = \left[\frac{7.27 r_t}{f^2 + 0.351 r_p^2 r_t^2} + \frac{7.5}{(f-5.7)^2 + 2.44 r_p^2 r_t^5} \right] \times \quad f^2 r_p^2 r_t^2 \cdot 10^{-3} \tag{5.19}$$

$$\gamma_w = \left[\begin{array}{l} 3.27 \times 10^{-2} \mathrm{r_t} + 1.67 \times 10^{-3} \frac{\rho_{\mathrm{r_t}}^7}{\mathrm{r_p}} + 7.7 \times 10^{-4} \mathrm{f}^{0.5} + \frac{3.79}{(\mathrm{f}-22.235)^2 + 9.81 \mathrm{r_p}^2 \mathrm{r_t}} + \cdots \\ \frac{11.173}{(\mathrm{f}-183.31)^2 + 11.85 \mathrm{r_p}^2 \mathrm{r_t}} + \frac{4.01_{\mathrm{r}} \mathrm{t}}{(\mathrm{f}-325.153)^2 + 10.44 \mathrm{r_p}^2 \mathrm{r_t}} \end{array} \right] \mathrm{f}^2 \rho \mathrm{r_p} \mathrm{r_t} \times 10^{-4} \tag{5.20}$$

Where:

$$\begin{aligned} \mathrm{rp} &= \mathrm{p}/1013 \\ \mathrm{rt} &= 288/(273 + \mathrm{T}) \end{aligned} \tag{5.21}$$

The variables atmospheric pressure (p) and temperature (T), which will be fixed values denoted in [31]; being 1013.25 hPa and 15ºC, respectively.

The equivalent height, h_w y h_o are described as follows [15]:

$$h_w = h_{w0} \left(1 + \frac{3}{(f-22.2)^2 + 5} + \frac{5}{(f-183.3)^2 + 6} + \frac{2.5}{(f-325.4)^2 + 4} \right) \tag{5.22a}$$

$$h_0 = 6, \text{ for f} < 50\text{GHz} \tag{5.22b}$$

Finally, as in previous sections, a Matlab function has been created, described below:

```
att  = gasAttenuation(freq,lat,lon,elev,p)
```

5.1.4.1 Variation in the percentage of an average year (p)

As we can see in figure 5.12, we have the same behaviour according to the band independently of the working band. We have a large attenuation with a low probability, together with a peak at 10%. Note that there is again a large difference between the attenuations depending on the frequency used, with more attenuation in the Ka-band. The available values of p are described in the table 5.2.

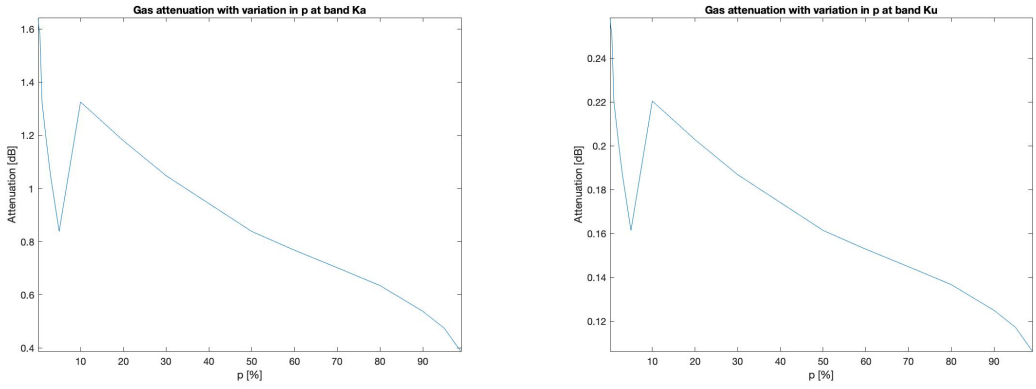

(a) (b)

Figure 5.12: Variation of the gas attenuation in function of p at bands Ka and Ku.

5.1.4.2 Variation in the frequency

About the variation in the frequency in the gas attenuation, we can observe a peak in the 22 to 24 GHz band, on the Ka band side; following the same behaviour as in previous points, obtaining a higher attenuation.

On the Ku band side, we can observe an increasing slope practically proportional to the frequency value. This is due to the fact that we have a peak around 20 GHz, therefore, working in this band, we will have lower attenuations. Anyway, the attenuation value is merely symbolic.

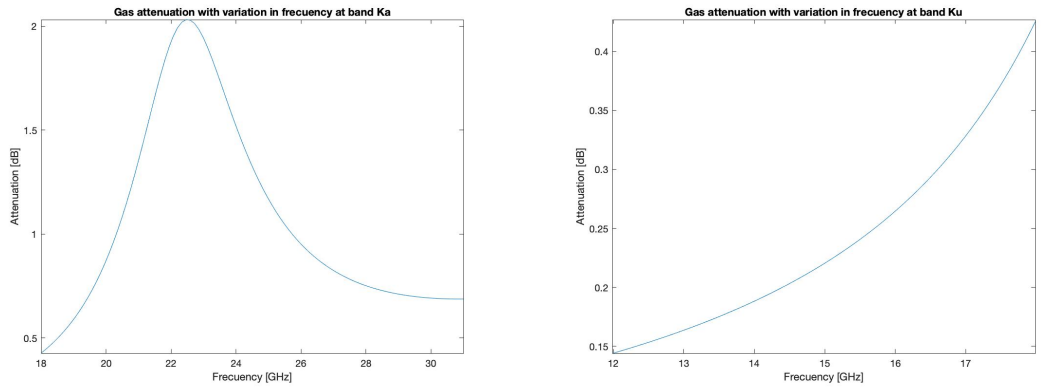

(a) (b)

Figure 5.13: Variation of the gas attenuation in function of frequency at bands Ka and Ku.

5.1.4.3 Variation in the longitude and latitude of the ground station

Finally, looking at the variation of latitude in figure 5.14, we can observe abrupt modifications of the attenuation at latitudes close to 20°.

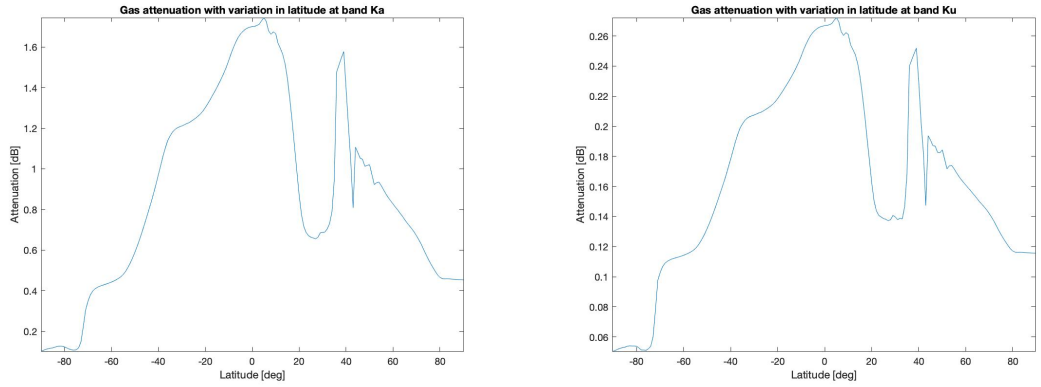

(a) (b)

Figure 5.14: Variation of the gas attenuation in function of latitude at bands Ka and Ku.

The variation in longitude, described in figure 5.15, indicates a very curious effect due to the fact that we have a practically constant attenuation over the entire globe, although the absolute value is considerably small. Comment on the fading on the part of the attenuation at longitudes around -75º and 40º.

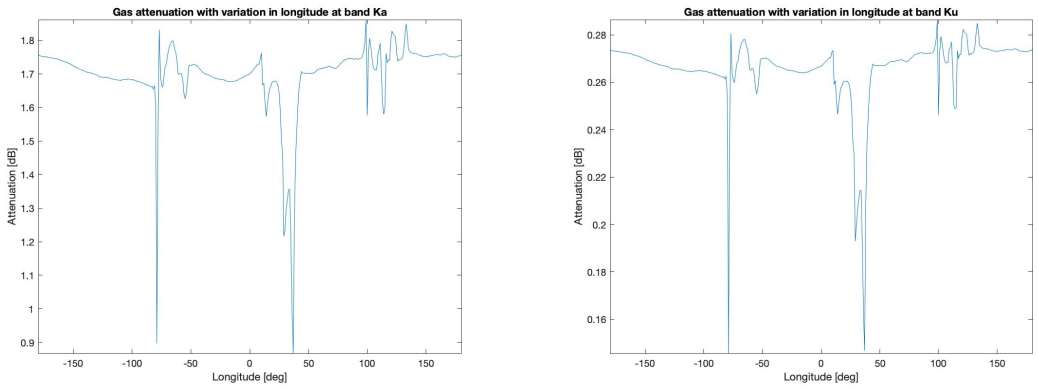

(a) (b)

Figure 5.15: Variation of the gas attenuation in function of longitude at bands Ka and Ku.

5.2 Scenarios

This section will show the real attenuation cases for each of the points described in the section 4.1, where the position of the earth station will now be of importance, since its climate will affect the total attenuations due to atmospheric phenomena. We must bear in mind that each of the climates chosen for the study have quite different characteristics, with variations in latitude and longitude in their position, taking into account the two hemispheres of the planet.

The following figures will show the total computation of attenuations included in previous sections. For easier comprehension, a list is added where we can quickly make the color and information pairs:

- Dark blue: Gas attenuation.
- Light blue: Cloud attenuation.
- Green: Rain attenuation.
- Yellow: Total attenuation.

Firstly, in the first point of interest, Barcelona, we can observe the following characteristics at the loss level, described in the figure 5.16 and 5.17. In those figures, we can observe a variation of the minimum elevation of the user antenna, described in a range from 10 to 55 degrees. It should be noted that the minimum value for a good communication is 40 degrees [19].

Barcelona is a coastal Mediterranean climate, and a large part of the losses are due to rainfall, increased by the value of the uplink frequency, given that it is a higher value. On the other hand, the losses due to clouds and gases, as we have seen in the sections 5.1.3 and 5.1.4, have little relevance in the total of our attenuation.

As we will be able to observe in the following of this study, the elevation of our ground station (i.e. antenna), will give us the ability to modify the attenuation as well.

Emphasizing this same parameter, and correlating the information obtained in [19], we can observe that the value of the total attenuation, although it has a certain variability, starts to be relatively constant from 30/35 degrees. Therefore, small modifications to the elevation of our user antenna will not have a major effect on the capabilities of the system.

Considering that the installation is up to the end user, these small differences can be created in the usual way; by obtaining an elevation higher than 35 degrees, this harmful effect on the system is then minimized.

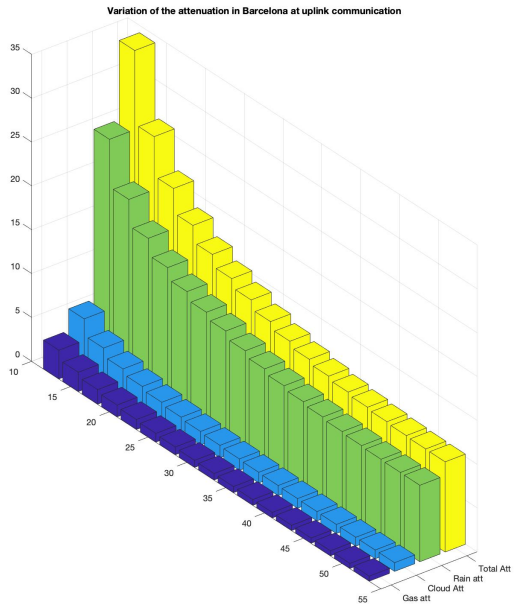

Figure 5.16: Variation of the attenuation in function of elevation in Barcelona in uplink.

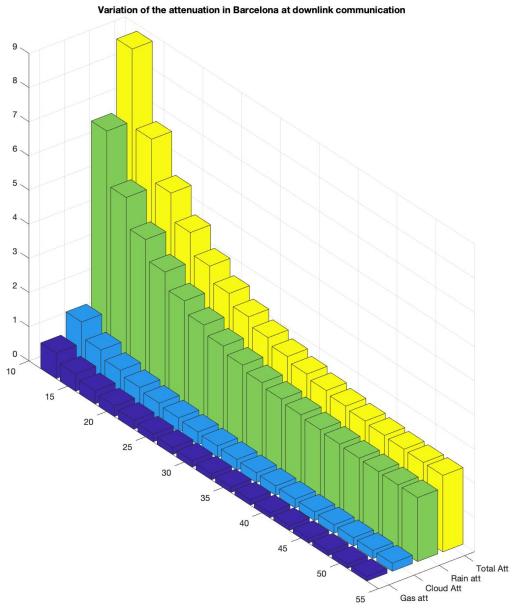

Figure 5.17: Variation of the attenuation in function of elevation in Barcelona in downlink.

Secondly, we will focus on figures 5.18 and 5.19 where we can see the same study on the Sao Paulo side, having the same variation on the minimum elevation side. This second scenario gives us the highest attenuations in the two communication links. As can be seen in the rain attenuation, it has a large contribution reaching almost 50 dB. This is due to the fact that one of the main cities in Brazil has a subtropical climate where we have rainfall at the extremes of the year.

As for the attenuation of gases, it still does not have much influence on our system, since in this second case, it is still the attenuation with the smallest contribution. Focusing on the cloud attenuation, given that we have a large attenuation by rain, the appearance of a higher value of this is obvious. This is because one of the factors that increases the cloud contribution is the total columnar content of reduced cloud liquid water (L_{red}), described in 5.16.

In addition, the same phenomenon should be commented on the variation of the total attenuation from a variation in elevation; due to the fact that we have a certain stabilization of the value from 35 degrees, this reaffirms for the second time the minimum elevation and its effect on the system.

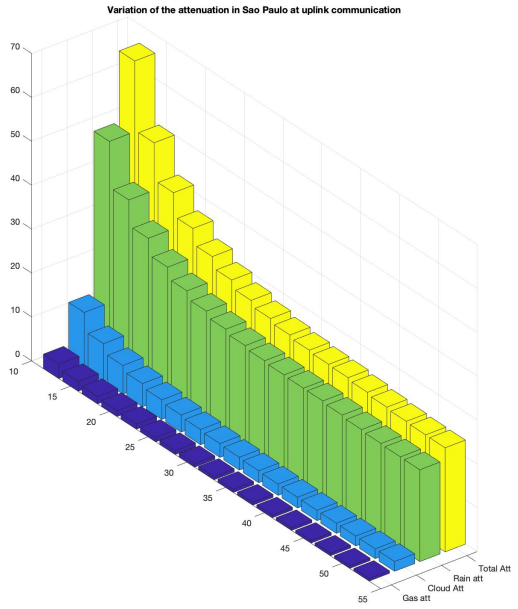

Figure 5.18: Variation of the attenuation in function of elevation in Sao Paulo in uplink.

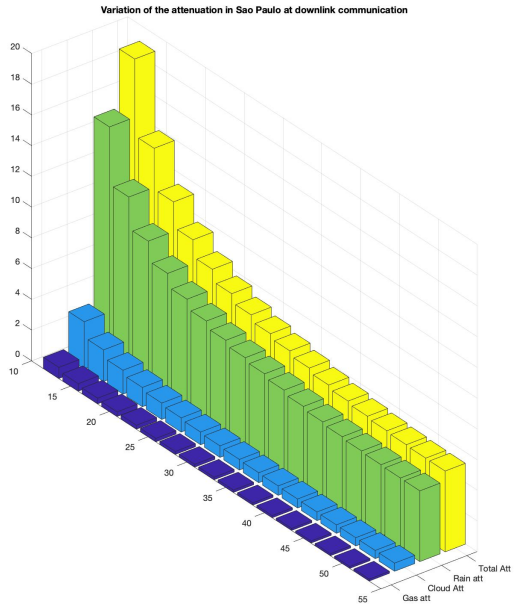

Figure 5.19: Variation of the attenuation in function of elevation in Sao Paulo in downlink.

Finally, we can observe in figures 5.20 and 5.21, the variation of the same attenuations for the Russian city of Moscow. This city has a humid continental climate with long winters

and mild, short summers. They have the great majority of their weather with cloudy days, a fact that we can easily relate to the data collected in the figure. In relation, the attenuation produced by clouds is the most outstanding of the three study points. On the other hand, rain attenuation continues to be the most important contributor, as in the previous cases.

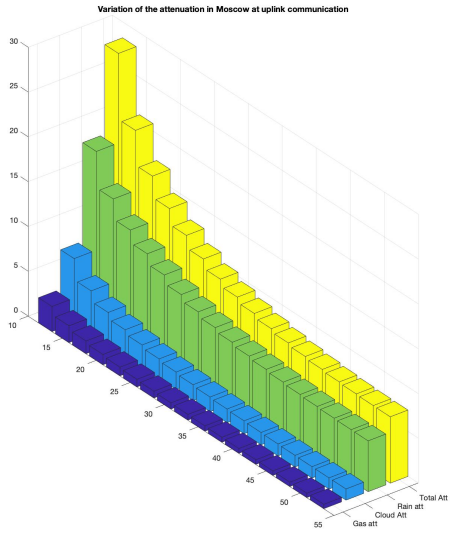

Figure 5.20: Variation of the attenuation in function of elevation in Moscow in uplink.

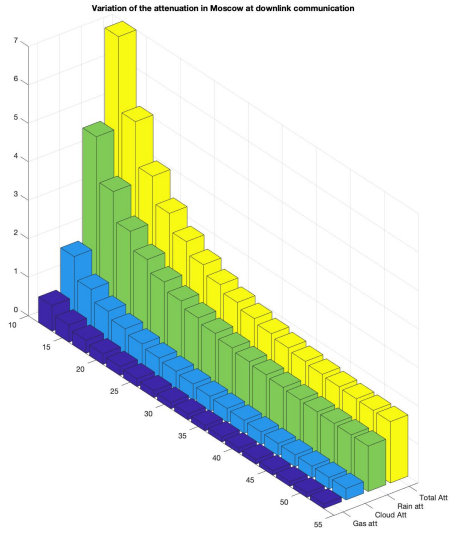

Figure 5.21: Variation of the attenuation in function of elevation in Moscow in downlink.

Another important point to study for our selected points is the average visibility time. For this purpose, the figure 5.22 is added where we can observe the mean time of all satellites, taking into account all satellites in the constellation at the moment. As in section 4.3, a whole day will be taken into account as visibility window. A higher average time visibility can be seen for central longitude values, such as the city of Barcelona. Next, we can observe how Moscow has a shorter mean visibility time and a lower number of visible satellites (see 4.1) having so the poor performance of our comparison with those parameters under study.

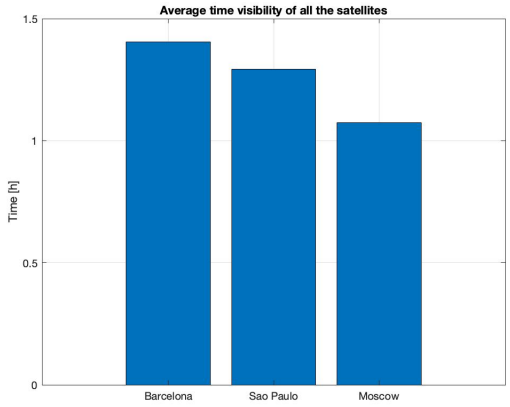

Figure 5.22: Average time visibility.

5.3 Capacity of the constellation

This section will show the constellation capacity, described in 3.3.4, as a function of the total visibility time of each of the visible satellites for each of the study points. Note that we will obtain the capacity within the visibility window described above in section 4.3, with a study value of 24 hours, although in the images described in this section they will be normalized to the satellite with the longest visibility time and therefore the longest trace length. On the X-axis, we will then have described a value of total samples of the vector of capacities of the different satellites.

For this purpose, a value of 40 degrees has been designated for the minimum elevation of our antenna, since, as we have seen in section 5.2, this value has a constant attenuation due to atmospheric phenomena, also mentioned in [19]. Following the thread of atmospheric losses, they have been calculated for a 99% feasibility; also for both uplink and downlink directions of the channel. The capacity value will be displayed in Mbits/s, given the large capacity of this system. The code for obtain this study is added in 3.3.4.1.

Therefore, in figure 5.23, we can observe the capacity of the visible satellites for the city of Barcelona. Note that we have most of the satellites within a small difference in capacity, where all of them have the same visibility time. These are the satellites that provide coverage within the space under study, as all of them are capable of providing coverage at any time of our connection.

Next, we can observe other satellites with greater capacity or greater visibility, although they are few in number. It is relevant to note that the capacity resulting from this study has a value similar to that added empirically by [19], as well as the fact that most satellites orbit above 550 kilometres, as mentioned in the introduction. Satellites outside this orbit obtain a different capacity than the nominal one, as could be the one we have with the highest capacity (being practically double that of fibre optics).

Therefore, we can say that in Barcelona, Elon Musk's expectations can be fulfilled given that theoretically, it has greater capacity than the conventional fibre optics that internet users can have right now in their private homes or businesses. Succeeding,

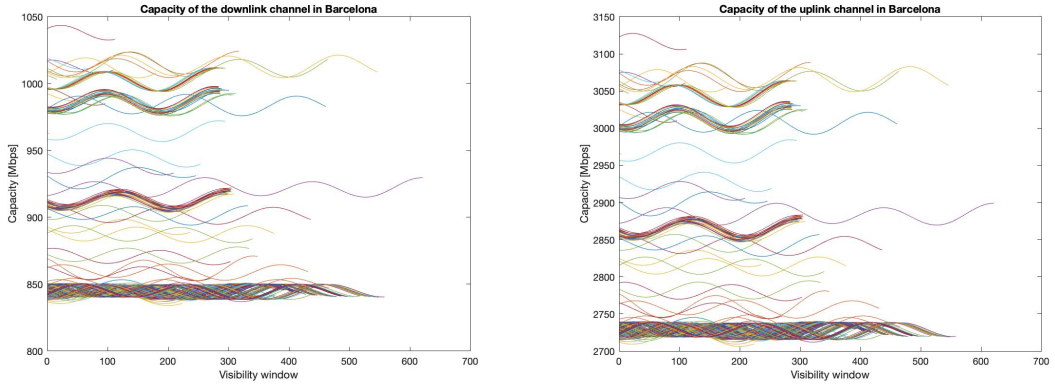

(a) (b)

Figure 5.23: Capacity of the constellation in Barcelona.

we plot the capacity of the constellation in Moscow, in the figure 5.24, noting that most satellites have the same capacity for the uplink and downlink links. It can be seen that the capacity at this point is higher than in the previous case. As we have been able to observe in the section 5.2, it has been the point of study with the lowest losses, therefore, where the Signal to Noise Ratio (SNR) will be higher. With a fixed bandwidth, it causes a considerable improvement in the final capacity of the system at this point. Note that there is the same behavior by the satellite with the highest capacity, which in turn has the shortest visibility time for the end user. The same conditions have been considered as in the previous case in terms of losses and antenna elevation.

As we have seen in the previous case, we have a higher capacity than fibre optic user, obtaining up to 30% more in downlink and up to 5 times more in uplink.

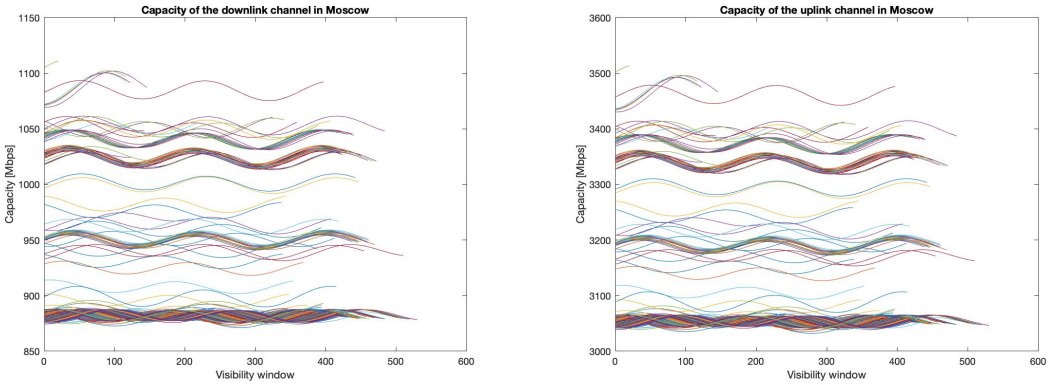

(a) (b)

Figure 5.24: Capacity of the constellation in Moscow.

At last, we have the figure 5.25, where is showed the capacity of the city of Sao Paulo. Contrary to the previous situation, in this case we had large losses associated with weather, with fewer satellites in visibility and together with a reduction in seeing time, seen in the section on 4.3.

Although we can observe a decrease in capacity, and therefore in data transfer with the satellite-user link, we can see that it still has great values, higher than the capacity of commercial fibre optics.

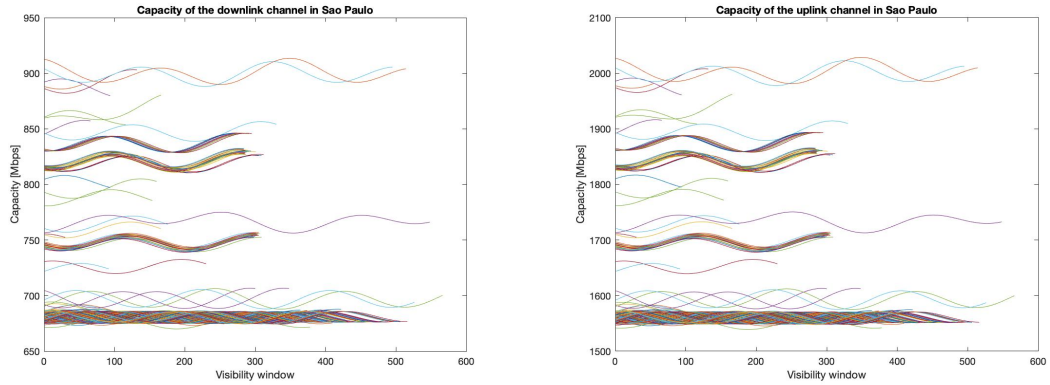

(a) (b)

Figure 5.25: Capacity of the constellation in Sao Paulo.

To conclude this part of the study, taking into account all the parameters studied, we can observe the behavior of the constellation in the northernmost city on Earth, which is

Alert, in Canada. In this case, we will only analyze the capacity obtained by the satellites visible from the ground station, maintaining the same probability and antenna elevation parameters as in the previous cases.

Next, we can observe in the figure 5.26 below the capacity of the satellites in question. In it we can observe a considerable reduction of the visible satellites, given its high latitude value, see figure 4.1, where we can observe that at the poles we do not obtain visible satellites, although being a somewhat lower value, the position is able to observe some of them.

On the visibility time side, being the length of the traces described in the figure 5.26, we can observe that the position of our ground station causes a reduction also in the total visibility time. Therefore, in a study window of one day, we obtain a visibility of less than one hour per satellite.

Finally, looking at the capacity of the satellites, we obtain a higher value than those described above, given that, as we have seen in the section 5.1.2 and the followings, in the extreme latitudes of our planet, we obtain practically no losses associated with the weather conditions. It has been considered that the power sent by the satellite and the gain remain the same, as described in [19], even though it is a very low visibility point.

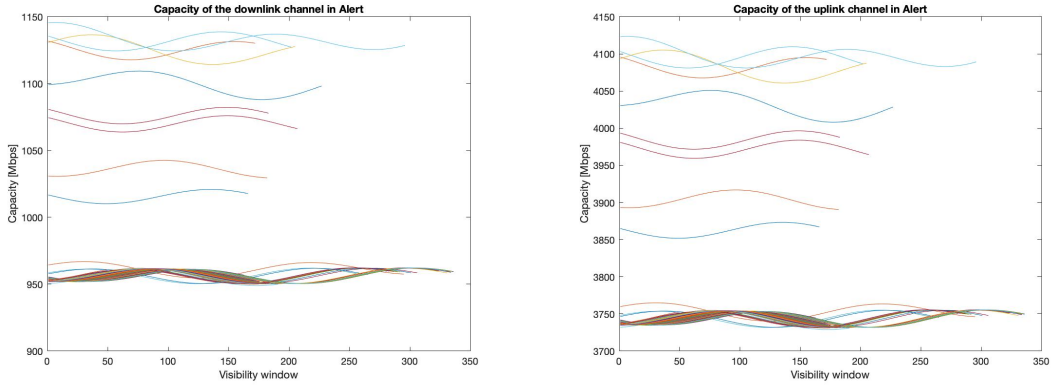

(a) (b)

Figure 5.26: Capacity of the constellation in Alert.

In conclusion, all the study points give higher experimental capacities than the fibre optic that can be contracted, although fibre optic internet could be up to 1 Gbit, causing the value obtained in this study to be somewhat lower in downlink.

Chapter 6

Conclusions

After the project is developed, several conclusions can be drawn from all the work performed. This chapter attempts to summarize what was learned while working on this thesis and the conclusions obtained.

Starlink is about a mega constellation that wants to bring internet capability to every place in the world, no matter how remote. This is a very tempting claim, especially given the situation we have right now, where the focus of the workspace is shifting completely, so that many jobs can now be remote.

In chapter the study objectives of this work were introduced and have been worked on in the different chapters of the project. Firstly, all the fields described in the TLE file have been obtained and understood. With them, we have been able to show the orbits where all the satellites of the constellation are, for the time being available.

Thanks to the values of the discrete positions of the satellites in their orbits, it has been possible to show the coverage of each of them given a terrestrial point. For this, the geometry behind the connections has been shown and it was observed that within a range of latitudes, described by the inclination of the satellites, we can observe good coverage for all of them. Continuing with the geometry issue, it is shown how to calculate the visibility window as a function of the degree of the ground station position and the difference between the longitudes of the two system elements. Finally, by correlating the values of the temporal window, together with the values of the previously discussed orbits, we can have the positional values where we observe the satellite correctly.

Once the positions were calculated, we proceeded to look at the losses associated with each of the study points, observing the climatic differences and therefore the

variation of attenuations by climate. This information gives us the ability to observe which positions will have more or less capacity, in the chapter 5, it is shown how these variations affect the frequency bands of use.

Finally, we arrive at the total capacity of the constellation, seeing that it is indeed able to obtain the promised values, even if the constellation is not complete. Looking at the different figures within the 5.3 section, we can conclude what has been pointed out throughout the project, that we will obtain consistent values within the areas where we have higher population density and therefore more potential customers to be able to get the Starlink pack. It is relevant to remember that the project behind this constellation is a pure business, where it should find the most potential customers.

Even so, we have been able to observe a very particular case, in Alert, Canada, where we have seen that we obviously have a considerably lower amount of visible satellites than the data from the previous cities, although we can have a part of the constellation that is able to create a radio communication link with the client. The visibility time is quite small, although it is fully compensated by the increase in capacity compared to the other points of interest; in this case, we observe that we have the highest capacity of our study, higher than described in [19] with a value of 2682.1 Mbps in the uplink budget and 674.3 Mbps for the downlink. Although the values described in this study, even if they seem really high, they are relatively small with the promises at the end of the construction of this constellation, given that a value of 17 to 23 Gbps in download is foreseen.

In addition, on Starlink's official website [34], we can see that the promises they show us are between 100 and 200 Mbps on average, with a peak of 700 Mbps; these values, although very different from our calculations, are totally inferior to those obtained mathematically by this study. Although they themselves have described that in download peaks, they will be able to obtain more than 600 Mbps, being somewhat similar to our calculations.

In conclusion, the Starlink constellation today is able to deliver the channel capacity it promises, giving good data transmission; this value will surely be improved in subsequent launches, occurring the completion of the deployment of the constellation.

Bibliography

[1] Mark A. Sturza,"The Teledesic satellite system: overview and design trades".

[2] Kris Maine, Carrie Devieux, Pete Swan,"Overview of IRIDIUM Satellite Network", AZ (EUA), 1995.

[3] Commercial IoT Coverage Map [Online], available: https://www.globalstar.com/es-es/coverage-maps

[4] Webinar: IoT de Dual Mode [Online], available: https://www2.orbcomm.com/satellite-cellular-iot-es

[5] OneWeb [Online], available: https://es.wikipedia.org/wiki/OneWeb

[6] Amazon's Project Kuiper makes steady progress, here are its antennae [Online], available: https://www.gizlogic.com/project-kuiper-amazon-hito/

[7] Li, Bofeng and Ge, Haibo and Ge, Maorong and Nie, Liangwei and Shen, Yunzhong and Schuh, H., "LEO enhanced Global Navigation Satellite System (LeGNSS) for real-time precise positioning services.", Advances in Space Research, 1998.

[8] Zehentner, Norbert,"Kinematic orbit positioning applying the raw observation approach to observe time variable gravity", 2017.

[9] G. Blarzino, L. Castanet, L. Luini, C. Capsoni and A. Martellucci, "Development of a new global rainfall rate model based on ERA40, TRMM, GPCC and GPCP products," 2009 3rd European Conference on Antennas and Propagation, 2009, pp. 671-675.

[10] Ramon Martinez Rodriguez-Osorio, Miguel Calvo Ramon,"Comunicaciones por satélite - Mecánica orbital", Madrid (Spain), 2009-2010.

[11] Ramon Martinez Rodriguez-Osorio,"Tipos de orbitas. Constelaciones de satélites", Madrid (Spain), 2009-2010.

[12] Shkelzen Cakaj, Bexhet Kamo, Algenti Lala, Alban Rakipi,"The Coverage Analysis for Low Earth Orbiting Satellites at Low Elevation", *(IJACSA) International Journal of Advanced Computer Science and Applications Vol.5, No 6*, 2014.

[13] W. Pritchard, H. Suyderhoud, and R. Nelson, Satellite Communication Systems Engineering. Prentice Hall, 1993. [Online], available: https://books.google.es/ books?id=8EjHQgAACAAJ

[14] Population density [Online], available: https://en.wikipedia.org/wiki/Population$_d$*ensity*

[15] Gataullin, Y., Kozlowski, R., "Implementation Of Rain And Gaseous Attenuation Models For 26-30 Gh Ka-Band Communication", *Proceeding of the 6th IASTED International Conference Antennas ,Radar and Wave Propagatiom* . Canada, 649-034.

[16] Abdulaziz Sultan Al-Ruwais, Abobakr Sultan Ahmed ,"Elevation-Angle Variation of LEO Satellites over the Kingdom of Saudi Arabia", *IArab Gulf Journal of Scientific Research, 26 (3): 145- 151*, 2008.

[17] "Space-X Non-geostationary satellite system, Attachment A"

[18] Càndia Muñoz Tardà,"Study of the ground to Very Low Earth Orbit (VLEO) satellite communication link", *Bachelor's Degree Thesis*, 2018.

[19] Inigo del Portilloa, Bruce G. Cameron, Edward F. Crawley,"A Technical Comparison of Three Low Earth Orbit Satellite Constellation Systems to Provide Global Broadband", 2021.

[20] Shkelzen Cakaj, Bexhet Kamo1, Algenti Lala, Alban Rakipi,"The Coverage Analysis for Low Earth Orbiting Satellites at Low Elevation", *(IJACSA) International Journal of Advanced Computer Science and Applications*, 2014.

[21] Celestrak, NORAD Two-Line Element Sets [Online],
available: https://www.celestrak.com/NORAD/elements

[22] Wikipedia, Two-line element sets [Online],
available: https://en.wikipedia.org/wiki/Two$_l ine_e lement_s et$

[23] Mathworks, Plot the orbit of a satellite [Online],
available: https://es.mathworks.com/matlabcentral/answers/499567-plot-the-orbit-of-a-satellite

[24] José L. CorralesGitHub [Online],
available: https://github.com/jlcorra/mfs3/tree/master/lib/tropos/src/%2Btropos

[25] Slideshare [Online],
available: https://es.slideshare.net/isabelasadobaysinaluisa/teledesic-1

[26] ESA, Types of orbits [Online],
available: https://www.esa.int/Enabling$_S upport/Space_T ransportation/Types_o f_o rbits$

[27] Meteoblue [Online],
available: https://www.meteoblue.com/en/weather/map/maxmintemp/world

[28] United States Department of Agriculture (USDA) - Global Population Density Map [Online]
available: https://commons.wikimedia.org/w/index.php?curid=490633

[29] Recommendation ITU-R P.840-6

[30] Recommendation ITU-R P.618-13

[31] Recommendation ITU-R P.618-13

[32] Recommendation ITU-R PN.837-1

[33] Recommendation ITU-R P.839.

[34] Starlink [Online],
available: https://www.starlink.com